スウェーデンハードロック研究所および超深地層研究所周辺領域の亀裂性岩盤を対象とした水理解析の実施

（核燃料サイクル開発機構 契約業務報告書）

2004年3月

三菱商事株式会社

2004年3月

スウェーデンハードロック研究所および超深地層研究所周辺領域の亀裂性岩盤を対象とした水理解析の実施

杉田 健一郎* William Dershowitz**

要旨

本報告書は、三菱商事株式会社が平成15年度に実施した、瑞浪超深地層研究所（MIU）計画並びにスウェーデンのHRL（Hard Rock Laboratory）国際共同研究である、エスポTRUE Block Scale Continuationプロジェクトに関わる作業を取り纏めたものである。

TRUE Bolck Scale Continuation（以下、TRUE-BSC）プロジェクトに関わる平成15年度の主要業務は、TRUE-BSに関わる試験計画、プロジェクトの前提条件の仕様、試験結果の解析及びトレイサーの水理試験の初期的なシミュレーションを支援することであった。

試験計画:TRUE-BSCプロジェクトにおいてプロジェクトの中で実施される予定のテストの前提条件を検討し、プロジェクトの目的に合致するよう試験要領を策定した。この試みは現存するテスト結果の解析と物質移行のシミュレーションの両方を含んでいる。

水力学影響分析:TRUE-BSCプロジェクトにおいて想定されている付加的な移行経路は付加的なストラクチャー#19に着目した水理テストによって平成15年度に特徴化された。水理試験解析曲線分析及び同時性分析を利用してこれらのテストの広範な分析が実施された。

流動及び物質移行のモデル化:TRUE-BS岩体を構成する亀裂の微小構造モデルのための水理構造モデルの開発を実施した。本モデルにおいては、角礫岩、断層粘土、カタクラサイト、マイロナイト、変質花崗岩から成る各不動帯の個別の特性が考慮された。平成15年度では個別のCPTシリーズ試験の為にシミュレーションが実施された。これらのシュミレーションはTRUE-BSCプロジェクトの最終テスト段階の設計を支援した。

MIUにおける主要業務は、たて坑の注入の影響に重きを置いたデータ分析及びMIUのたて坑の建設に関する水理構造のシミュレーションに集中された。

*MIZ及びMSBテスト解析支援：*水理試験解析コードFlowDimを用いてMIZ-1及びMSB試験の非整数次元解析を実施した。これら瞬間的な水理学的反応の分析は同時性（干渉）及び水理試験解析曲線分析が使用された。それぞれの試験においては、流動要因、伝導T、貯蔵性S、拡散性ηが計算された。

*MIUの水理構造学的な統合化：*MIUサイトの亀裂及び断層の幾何学及び特性をJCNがより一層理解を深めるために分析を実施した。

*亀裂ネットワーク・モデルの構築：*たて坑掘削から想定される水理学的影響のシミュレーションをMIUサイトのDFNモデルにて実施した。このモデルは亀裂の注入された部分にある亀裂の構成の減少の直接的なシミュレーションを通した注入影響が含まれている。

---

* 三菱商事株式会社

** Golder Associates Inc.

EXECUTIVE SUMMARY

During Heisei-15, Golder Associates provided support for JNC Tono at the MIU Underground Rock Laboratory and the Äspö Block Scale Continuation Project.

Major activities in support of the TRUE Block Scale Continuation project during H-15 were related to assistance in design of experiments and specification of project hypotheses, interpretation of experimental results, and preliminary simulation of tracer and hydraulic experiments.

Experimental Design: Golder worked with the TRUE-BSC project to develop the hypotheses to be tested during the project, and to select the experimental configuration most likely to meet project objectives. This effort included both interpretation of available in situ test results and solute transport simulation.

Hydraulic Interference Analysis: The additional pathways to be considered in the Block Scale Continuation project were characterized during H-15 by additional hydraulic tests focusing on structure #19. Golder Associates carried out an extensive analysis of these tests, using methods of fractional dimension type curve analysis and synchronicity analysis.

Flow and Transport Modeling: Golder developed and implemented an updated hydrostructural model for the microstructural model for fractures which make up the TRUE rock block. This model considers the individual properties of each immobile zone, including breccia, gouge, cataclasite, mylonite, and altered granite. During H-15, simulations were carried out for each of the CPT series of experiments. These simulations supported the design of the final testing phase of TRUE-BSC.

Major activities for the MIU Laboratory concentrated on data analysis, and simulation of hydrostructural response to the construction of the MIU shaft, with emphasis on the effect of shaft grouting.

MIZ and MSB Test Interpretation Support: The FlowDim fractional dimension hydraulic test interpretation system was used to carry out a unified analysis of the MIZ-1 and MSB experiments. These analyses of transient hydraulic responses used synchronicity (interference)

and fractional dimension type curve analysis. For each test, the flow dimension, transmissivity T, storativity S, and diffusivity η were calculated.

MIU Hydrostructural Synthesis: Analyses were carried out to help JNC develop an improved understanding of the geometry and properties of fractures and faults at the MIU site.

MIU Discrete Fracture Network Model: Golder implemented a DFN model of the MIU site for simulation of the hydraulic response to be expected from shaft sinking. The model includes the effect of grouting through a direct simulation of the reduction in fracture transmissivity in grouted portions of fractures.

TABLE OF CONTENTS

LIST OF TABLES

LIST OF FIGURES

1. INTRODUCTION

During fiscal year H-15, Golder Associates assisted JNC with hydrogeologic analyses and simulations for the MIU Underground Rock Laboratory and the Äspö Block Scale Continuation experiments. Support for the MIU Underground Rock Laboratory was focused on data analysis and simulation of hydraulic interference response to shaft construction. Äspö Block Scale Continuation efforts were focused on support to experimental design and test interpretation.

H-15 tasks are summarized in Table 1-1. H-15 Deliverables are summarized in Table 1-2.

Table 1-1 Heisei-15 Task Summary

Task	Title
1	Äspö TRUE Block Scale Continuation Project
2	MIU Project Discrete Fracture Analysis

Table 1-2 Heisei-15 Deliverables

Task	Title	Deliverable	Date
1.1	TRUE BSC Experiment Design	Report	Sept. 30, 2003
1.2	TRUE BSC Experiment Interpretation	Preliminary report Final Report	Dec. 26, 2003 Mar 12, 2004
2.1	MIU Hydraulic Test Interpretation	Report	Sept. 30, 2003
2.2	MIU Hydrostructural Synthesis	Report	Dec. 26, 2003
2.3	MIU DFN Modeling	Report	Dec. 26, 2003

2. ÄSPÖ BLOCK SCALE CONTINUATION SUPPORT

During H-15, Golder Associates supported JNC/Tono participation in the international TRUE Block Scale Continuation Project at Äspö, Sweden. The purpose of the TRUE Continuation Project is to enhance understanding of flow and transport processes in fractured rock at the 50 to 200 m scale, the key scale for repository safety assessment within the JNC repository safety assessment framework. JNC has participated in the TRUE Block Scale since 1998, and has played a key role in hydrostructural model development, experimental design, test interpretation, and numerical modeling.

Golder supported JNC during H-15 through two tasks:

- Task 1.1: Experimental Design
- Task 1.2: Experimental Interpretation

2.1 Task 1.1: Experimental Design

During H-15, the TRUE Block Scale Continuation Project (TRUE-BSC) designed tracer and hydraulic interference experiments to meet the project goals to improve understanding of flow and transport in fracture networks.

During H-15, Golder Associates assisted JNC in carrying out analyses and simulations to support experimental design, and preliminary predictive simulations for sorbing tracer pathways identified as the focus for the experiment.

2.1.1 Experimental Design Support

To support experimental design, Golder calculated "virtual packer" for the BS2B experimental configuration. Virtual packers are necessary because the actual intercepts between hydrostructural features frequently do not lie on a single plane, as would be predicted by models which assume that all structures are planar. "Virtual packers" are defined to be in the same approximate location along the borehole as the actual packer, but to include the hydrostructural features which are intersected by the actual boreholes.

Virtual Packers are shown in Table 2-1. These packers were calculated by first determining the intersections between hydrostructural features and the packers in the BS2B experimental array. Then, the packer locations along the model boreholes were adjusted such that the

hydrostructural features as specified in the reference hydrostructural model intersect the correct packer intervals.

Golder also calculated the fracture intersection geometries for Structure #19, which was selected as the focus for experiments in the BS2B phase. The fracture intersection geometry for Structure #19 is shown in Figure 2-1.

Table 2-1 Virtual Packers

KI0025F03	P-setting	Collar		Pkr10		#7	Pkr9		#6	Pkr8		#23	Pkr7		#22	Pkr6		#20	Pkr5			Pkr4		#21	Pkr3		#13	Pkr2		Pkr1		#19	END
		0		2.6	3.58	42.176	49.00	50.00	50.304	54.08	55.08	56.6	58.58	59.58	60.933	65.58	66.58	73.88	74.08	75.08		80.00	81.00	82.07	88.08	89.08	90.23	92.58	93.58	####	####	131.3	141.7
KI0025F02	P-setting	Collar		Pkr10		Pkr9		#7	Pkr8		#6	Pkr7		#23	Pkr6		#22	Pkr5		#20	Pkr4		Pkr3		#13	#21	Pkr2		#19	Pkr1		#10	END
		0		2.4	3.4	37.5	38.5	42.574	50.7	51.7	53.321	55.1	56.1	59.2	63	64	67.07	72.3	73.3	77.25	77.5	78.5	92.4	93.4	95.07	95.9	99.3	100	137.1	138	139	157.2	204
KI0023B	P-setting	Collar		Pkr9		Pkr8		#7	Pkr7		#6	#23?	#20	Pkr6		#21	Pkr5		Pkr4		#13	Pkr3		Pkr2		#19	Pkr1		#10	END			
		0		3.6	4.6	40.45	41.5	41.813	42.45	43.45	45.798	52.6	69.3	69.95	70.5	70.66	72	72.95	83.8	84.8	85.79	86.2	87.2	110	111	112.7	113	114	169.5	201			
KA2563A	P-setting	Collar		Pkr7		Pkr6		Pkr5		Pkr4		#7	#6	#22?	#21?	Pkr3		#20	Pkr2		#13	#19	Pkr1		END								
		0		5	6	75	76	112	113	145	146	150.85	154.7	141.69	171.20	186	187	186.25	196	197	205.3	229.6	265	266	362								
	R-setting	Collar		Pkr8		Pkr7		#7	#6	#22?	#21?	Pkr6		#20	Pkr5		#13	Pkr4		Pkr3		Pkr2		#19	Pkr1		END						
		0		75	76	145	146	150.85	154.69	141.69	171.20	186	187	186.25	190	191	205.3	219	220	224	225	228.0	229	229.6	261.0	262	362						
	S-setting	Collar		Pkr8		#7	#6	#22?	#21?	Pkr7		#20	Pkr6			Pkr5		#13	Pkr4			Pkr3		#19	Pkr2		Pkr1			END			
		0		145	146	150.85	154.7	141.69	171.20	185	186	186.25	190	191		204	205	205.28	208	209		####	228	229.6	241	242	246	247		362			
KI0025F	P-Setting	Collar	Pkr7		#7	Pkr6		#6	Pkr5		#20	#22	Pkr4		#13	Pkr3		Pkr2		#19	#21	Pkr1		END								
		0	2.5	3.5	39.45	40	41	61.813	85	86	86.757	88.597	89	90	109.46	151	152	157	158	163.6	167.1	168	169	194								
	R-setting	Collar		Pkr6		#7	Pkr5		#6	Pkr4		#20	#22	Pkr3		#13?	Pkr2		#19	#21	Pkr1		END								
		0		2.5	3.5	39.447	40	41	61.813	85	86	86.757	88.6	89	90	109.5	160	161	163.6	167.1	168	169	194								
	S-setting	Collar		Pkr6		#7	Pkr5		#6	Pkr4		#20	#22	Pkr3		#13?	Pkr2		#19	#21	Pkr1		End								
		0		4	5	39.447	41.5	42.5	61.813	85.5	86.5	86.757	88.6	89.5	90.5	109.5	160	161	163.6	167.1	170	171	194								
KA2511A	P-setting	Collar		Pkr4		Pkr3		#7	Pkr2		#6	#20?	#22?	#13?	#19?	#21?	Pkr1		#10	END												
		0		5	6	30	31	36.542	80	81	87.502	120.23	129.9	148.43	153.93	156.1	170	171	240	293												
	R-setting	Collar		Pkr6		#7	Pkr5		#6	Pkr4		#20?	#22?	Pkr3		#13?	#19?	#21?	Pkr2		Pkr1		#10	END								
		0		5	6	36.542	63	64	87.502	91	92	120.23	129.9	138	139	148.4	153.9	156.1	170	171	230	231	240	293								
	S-setting	Collar	#7	Pkr7		Pkr6		#6	Pkr5		Pkr4		#20?	#22?	#13?	#19?	#21?	Pkr3		#10	Pkr2		Pkr1		END							
		0	36.54	51	52	54	55	87.502	91	92	109	110	120.2	129.87	148.43	153.9	156.1	216	217	240	241	242	244		293							
	T-setting	Collar		Pkr8		#7	Pkr7		#6?	Pkr6		Pkr5		Pkr4		#20?	#22?	Pkr3		#13?	#19?	#21?	Pkr2		Pkr1		#10	END				
		0		5	6	36.542	64	65	87.502	95	96	102	103	110	111	120.2	129.9	138	139	148.4	153.9	156.1	170	171	238	239	240	293					

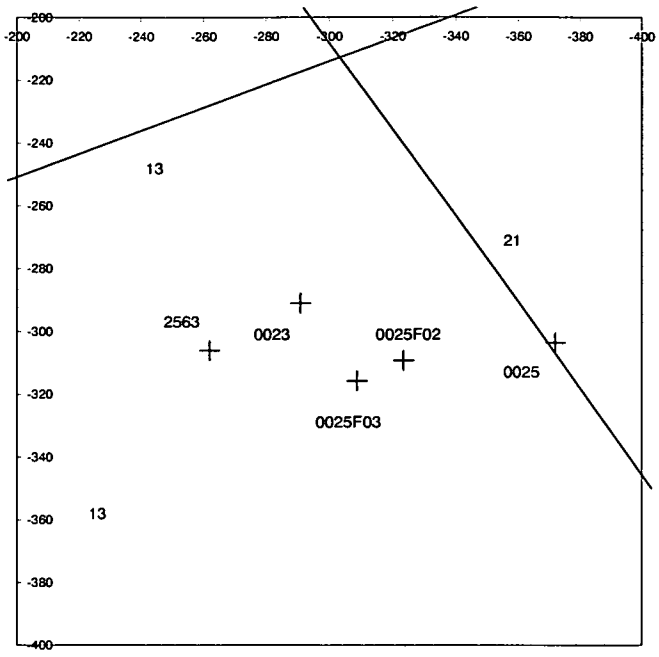

Figure 2-1 Fracture Intersections with Structure #19

2.1.2 Predictive Simulations

The predictive simulation was carried out for the proposed sorbing tracer test CPT-4. This simulation utilized the DFN model developed in Task 1.2, and described below. Here the tracer predictive simulation is described.

As described in the data delivery, experiment CPT-4 is being designed to target Structure #19 using various test geometries with KI0025F03 section R3 as the sink. The simulations are illustrated in Figure 2-2 and Figure 2-3. Table 2-2 lists the predicted characteristic times and recoveries for test CPT-4.

The recovery and breakthrough curves predict early recovery for Source 1 (KI0025F02:R3) and Source 2 (KI0023B:P2) which are located at relatively short distances from the sink (19.5 and 27 meters, respectively). For the longer path scenarios of 49 meters (Source 4 and Source 5), recovery times are much longer. For Source 4 (KA2563A:S1) 50% of the tracer is recovered at approximately 1400 hours and for Source 5 (KA2563A:S2) 95% recovery is not achieved until after 2100 hours (Table 2-2).

An interesting recovery feature is predicted for the Source 4 scenario (KA2563A:S1). The breakthrough curve suggests two peaks in mass flux at approximately 20 and 500 hours (Figure 2-3). The description of the proposed experiments in the data delivery document characterizes test scenario Source 4 as "dual intercept, mixing with source 5".

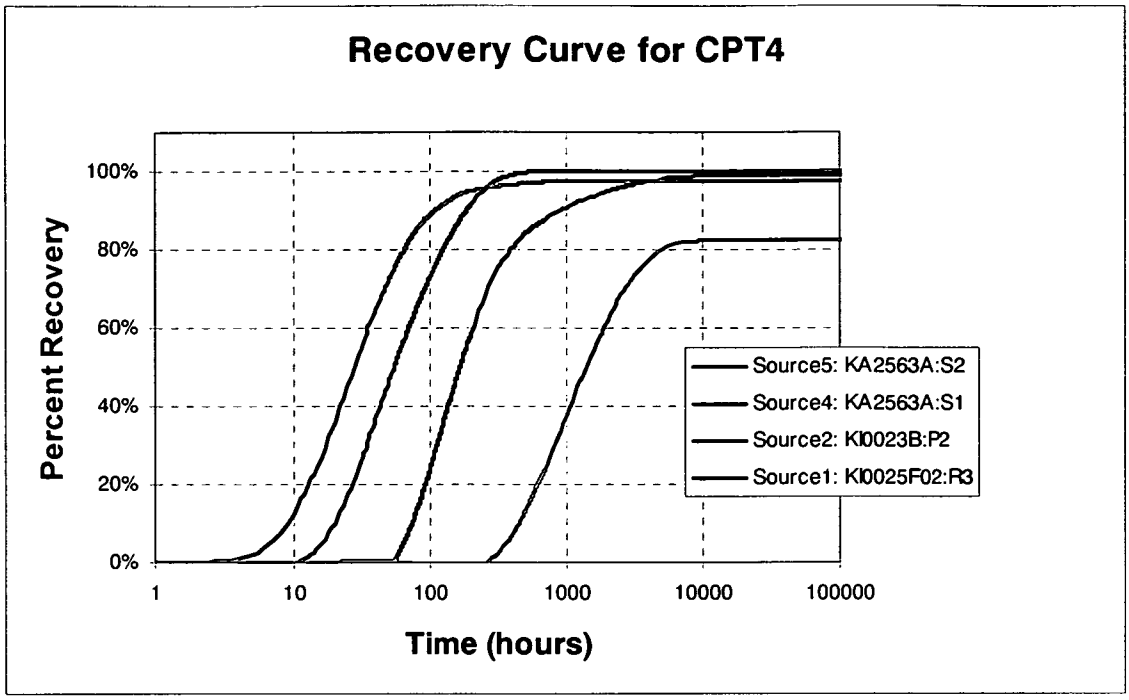

Figure 2-2 Predicted cumulative recovery curves for Rhenium, test CPT-4.

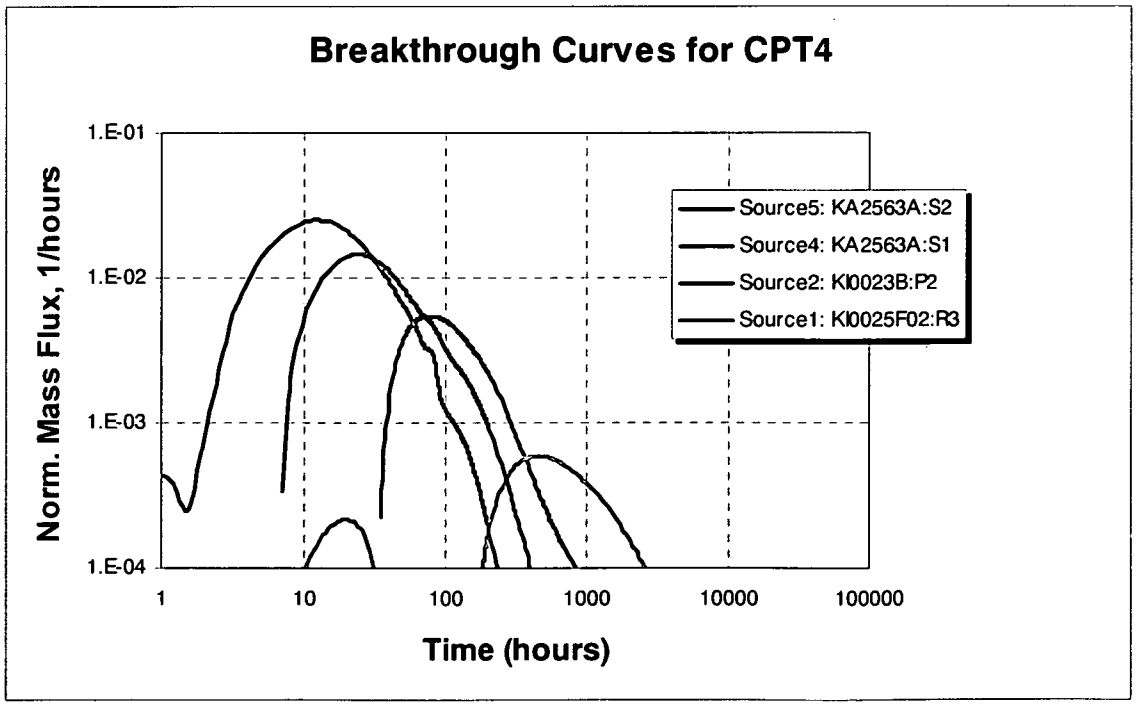

Figure 2-3 Predicted breakthrough curves for Rhenium, test CPT-4

Table 2-2 Predicted characteristic times (in hours) and total recovery at 10,000 hours for test CPT-4, non-sorbing Rhenium tracer

Metric	Source1	Source2	Source4	Source5
T_5	16.04	7.00	369.93	65.04
T_{50}	54.96	27.96	1402.56	165.68
T_{95}	249.83	198.99	N/A	2103.84
Recovery @10K Hrs	100.0%	97.5%	82.3%	98.9%

Sorbing nuclide tracers:

Additional tracer simulations were run under the CPT4 scenario but this time using sorbing nuclides Na-22, Ca-45, Sr-85, and Sr-90. The results suggest longer recovery times and slightly less overall recovery when compared to the non-sorbing tracer simulation (Figure 2-4 through Figure 2-7; Table 2-3 through Table 2-6).

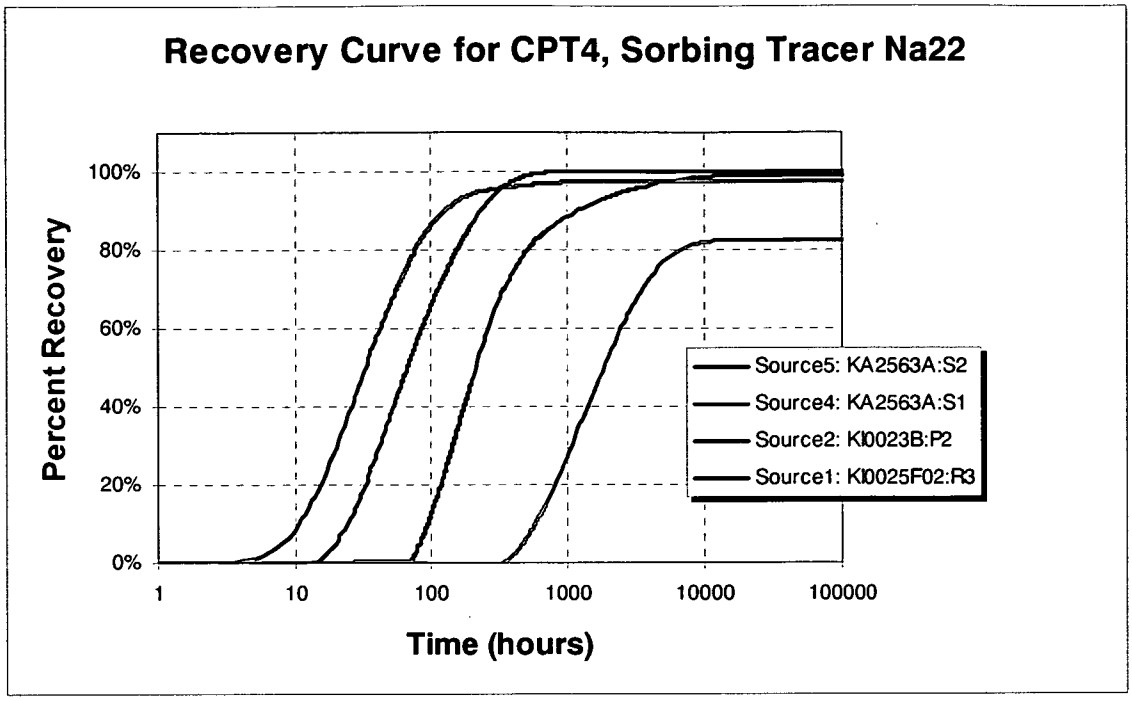

Figure 2-4 Predicted cumulative recovery curves for Na-22, test CPT-4

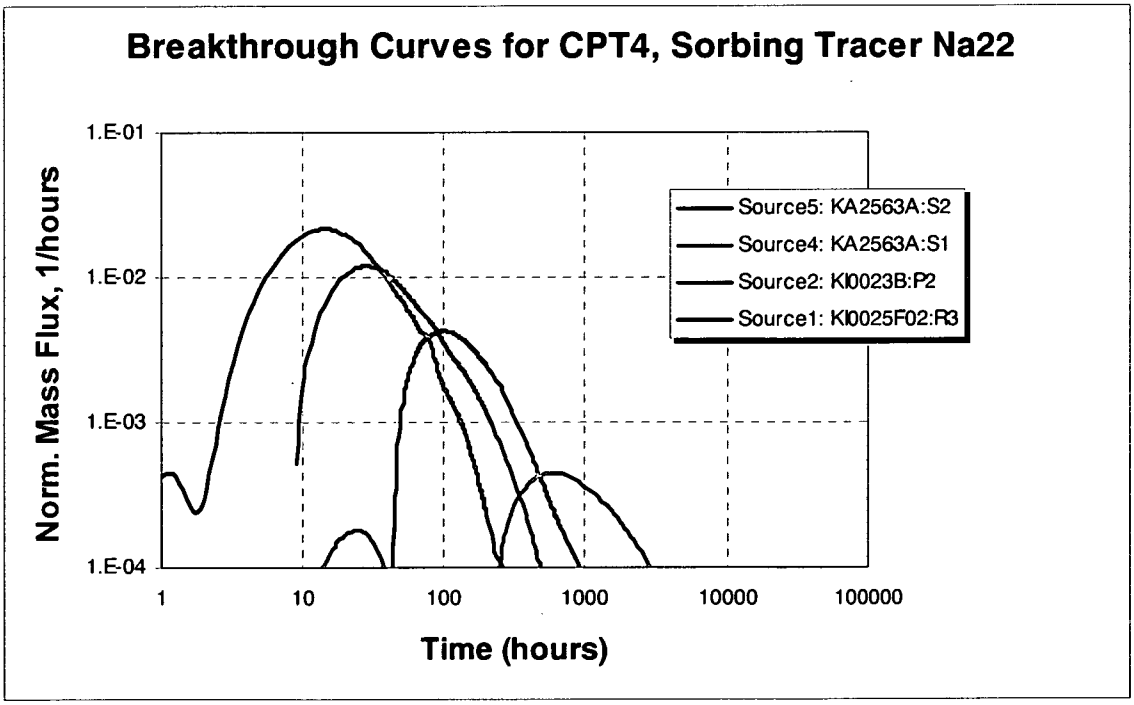

Figure 2-5 Predicted breakthrough curves for Na-22, test CPT-4

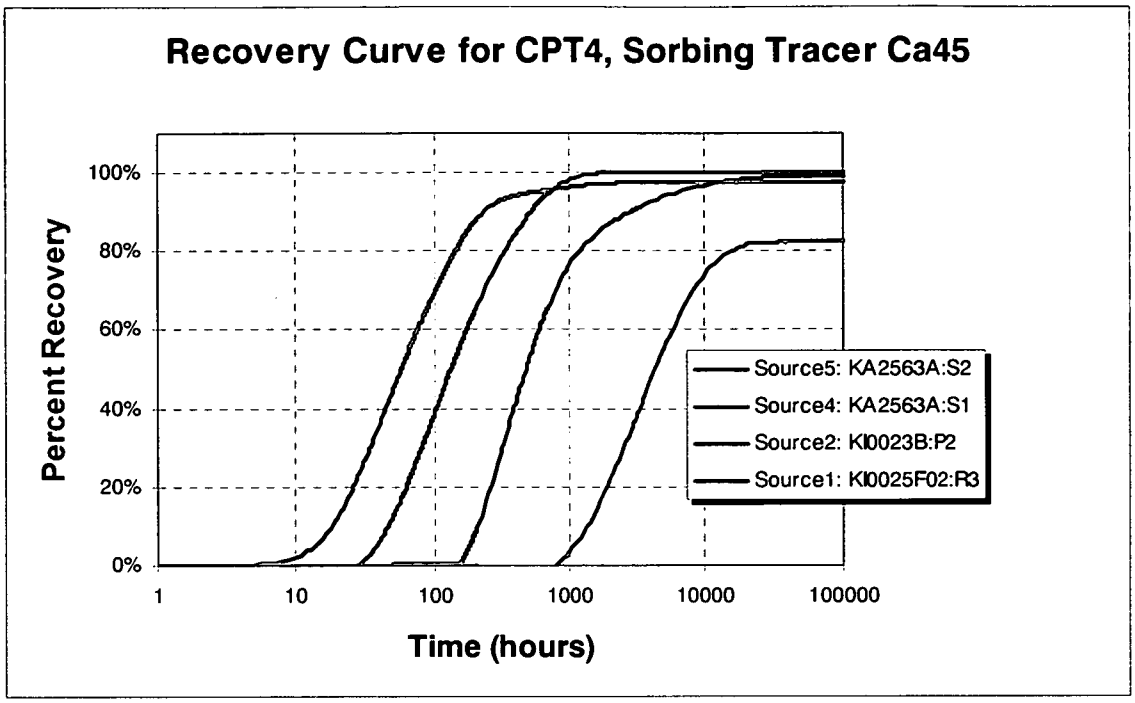

Figure 2-6 Predicted cumulative recovery curves for Ca-45, test CPT-4

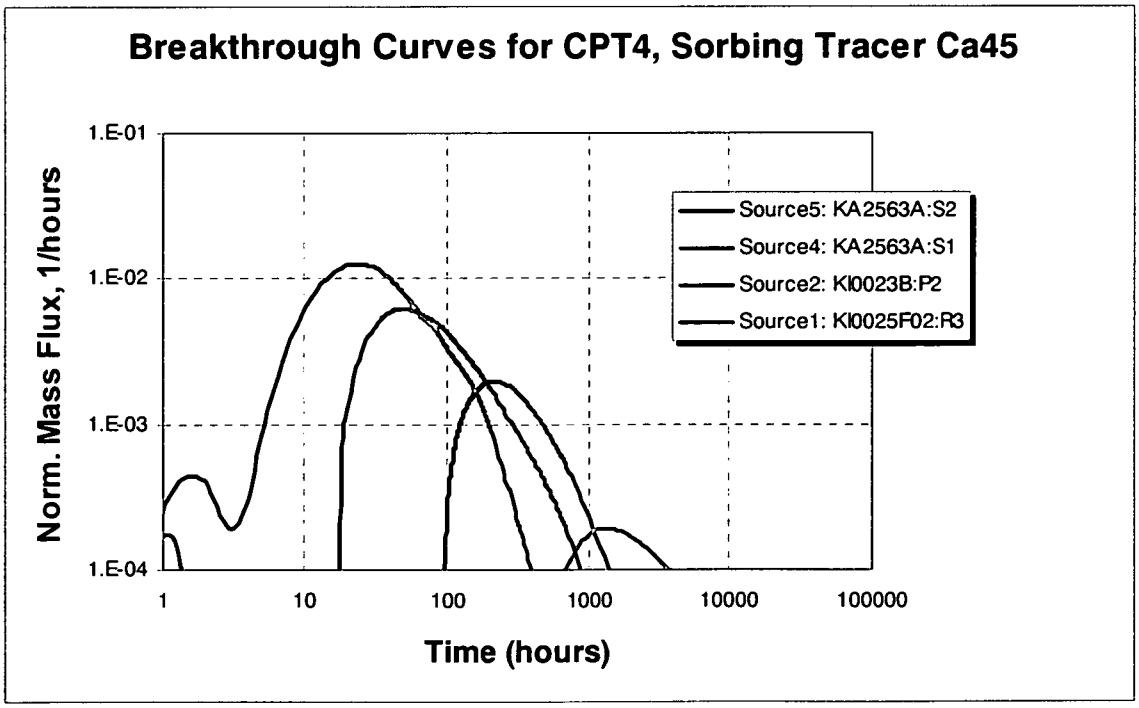

Figure 2-7 Predicted breakthrough curves for Ca-45, test CPT-4

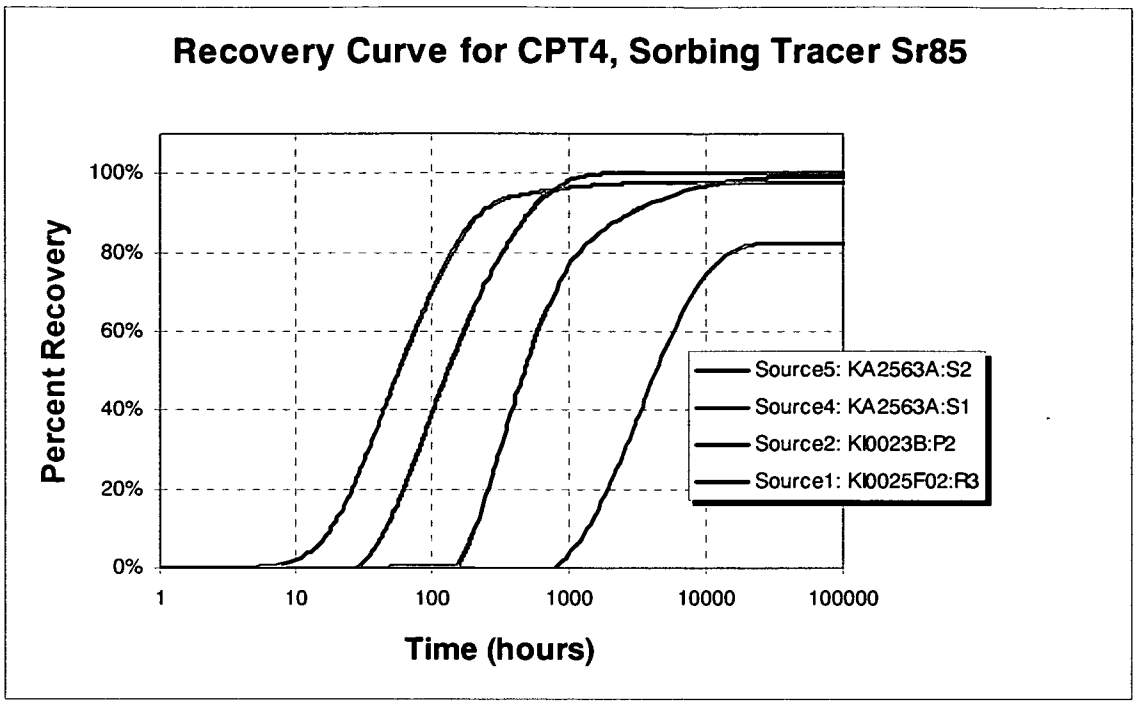

Figure 2-8 Predicted cumulative recovery curves for Sr-85, test CPT-4

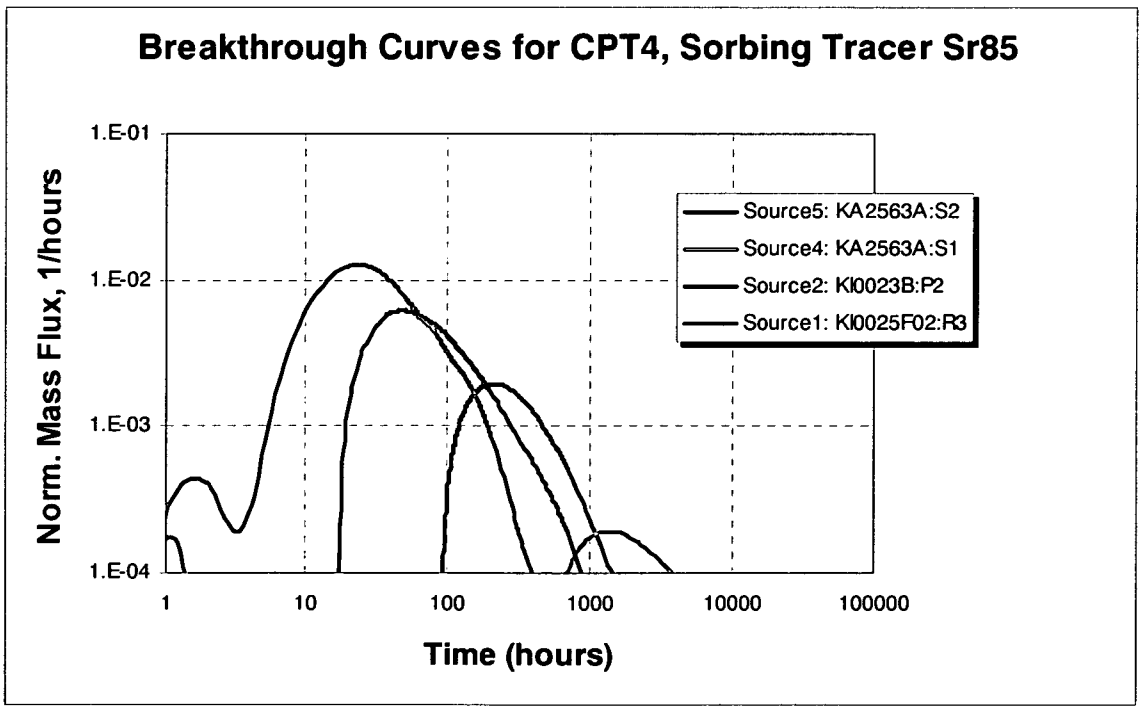

Figure 2-9 Predicted breakthrough curves for Sr-85, test CPT-4

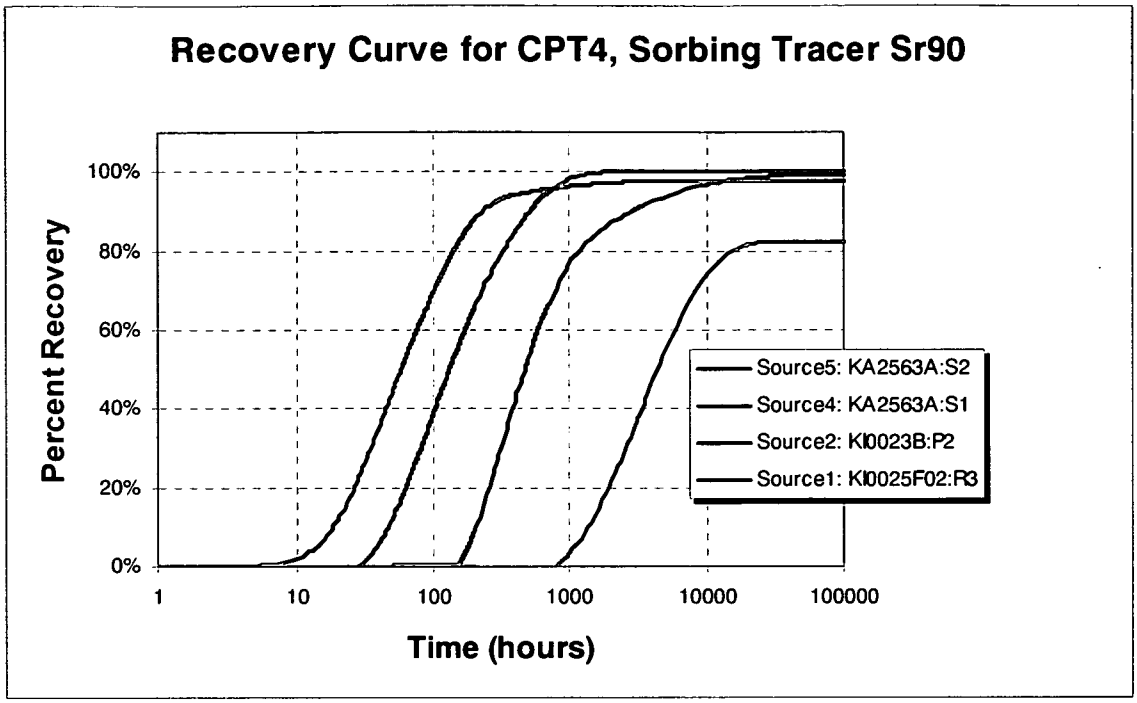

Figure 2-10 Predicted cumulative recovery curves for Sr-90, test CPT-4.

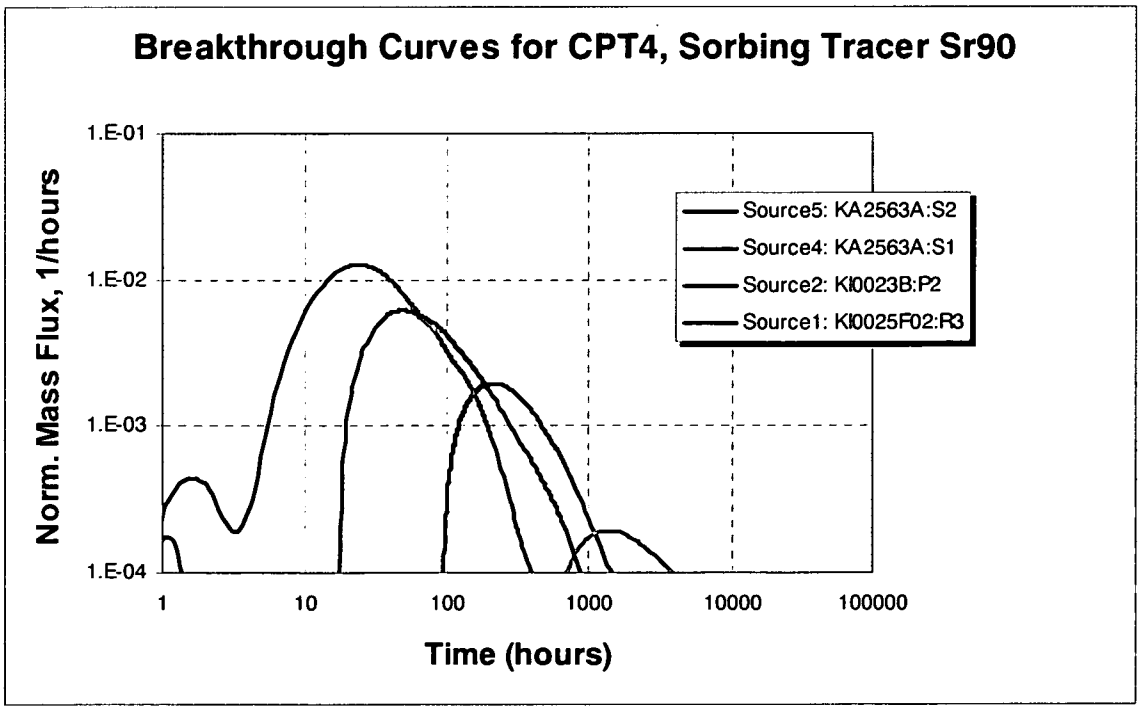

Figure 2-11 Predicted breakthrough curves for Sr-90, test CPT-4

Table 2-3 Predicted characteristic times (in hours) and total recovery at 10,000 hours for test CPT-4, sorbing tracer Na-22

Metric	Source1	Source2	Source4	Source5
T_5	19.9	8.0	480.4	82.9
T_{50}	68.0	32.9	1902.2	215.0
T_{95}	319.9	240.2	N/A	2750.0
Recovery @10K Hrs	100.0%	97.5%	82.4%	98.6%

Table 2-4 Predicted characteristic times (in hours) and total recovery at 10,000 hours for test CPT-4, sorbing tracer Ca-45

Metric	Source1	Source2	Source4	Source5
T_5	39.0	14.0	1095.0	180.6
T_{50}	134.1	58.5	4496.0	470.0
T_{95}	725.0	540.0	N/A	6500.0
Recovery @10K Hrs	100.0%	97.5%	82.4%	96.8%

Table 2-5 Predicted characteristic times (in hours) and total recovery at 10,000 hours for test CPT-4, sorbing tracer Sr-85

Metric	Source1	Source2	Source4	Source5
T_5	39	14.0	1095	181
T_{50}	134.0	58.5	4496.0	470.0
T_{95}	725.0	540.0	N/A	6500.0
Recovery @10K Hrs	100.0%	97.5%	82.4%	96.8%

Table 2-6 Predicted characteristic times (in hours) and total recovery at 10,000 hours for test CPT-4, sorbing tracer Sr-90

Metric	Source1	Source2	Source4	Source5
T_5	39.0	14.0	1095	181
T_{50}	134	58.5	4496.0	470.0
T_{95}	725.0	540.0	N/A	6500.0
Recovery @10K Hrs	100.0%	97.5%	82.4%	96.8%

2.2 Task 1.2 Experimental Interpretation

Within the TRUE BSC project, the JNC team plays a major role in experimental interpretation, particularly in development of hydrostructural models. During H-15, Golder provided support to

JNC in experimental interpretation for experiments carried out as part of the TRUE BSC project. This activity included the following:

- Analysis of Transient Hydraulic Data
- Analysis of Dilution and Tracer Tests
- Model Calibration Simulations
- Hypothesis Testing
- Reporting

2.2.1 Analysis of Transient Hydraulic Data

Golder carried out a detailed analysis of transient hydraulic test data to support the evaluation of Structure #19, the focus of planned TRUE-BSC sorbing tracer testing. This analysis used an approach similar to that developed for Structure #20 during the TRUE-BS project (Doe, 2003). The analysis provides insight on conducting geometry for evaluation of tracer tests and structural models.

The hydraulic data analyzed came from test CPT-3. The test results are provided in Figure 2-12. The analysis proceeded as follows. The hydraulic behavior of the fracture networks connected to the tested section is expressed through the time variation in the derivative dp/dt. By assuming diffusivity $\eta = 5\ m^2/s$, the derivative can be plotted as transmissivity (m^2/s) vs. distance from the hydraulic signal (m). This plot is shown in Figure 2-13.

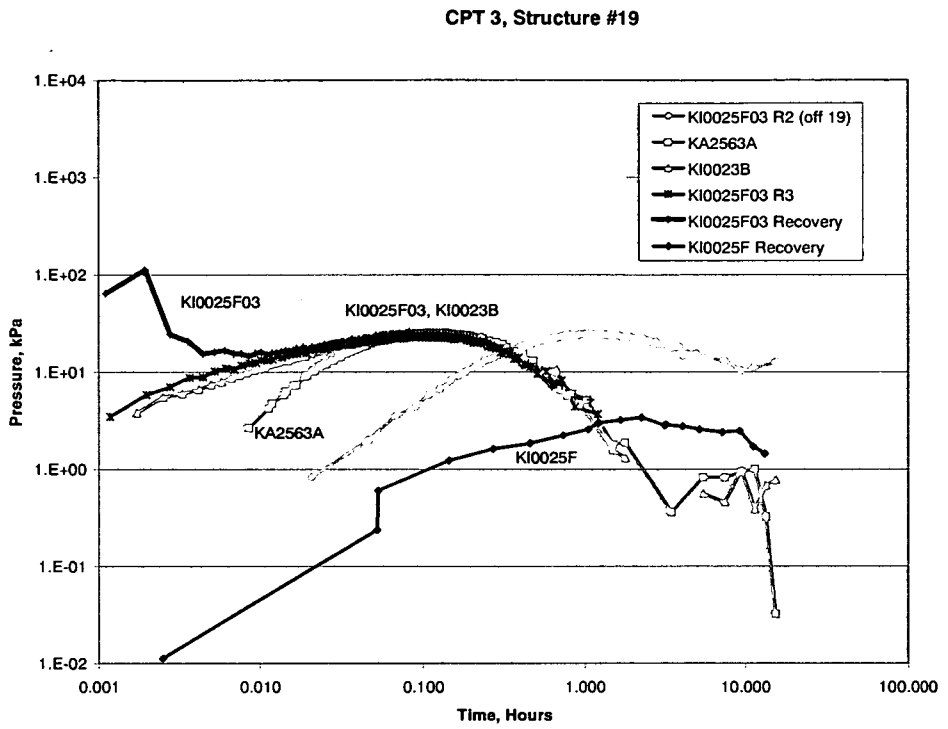

Figure 2-12 Hydraulic Test CPT-3, Structure #19

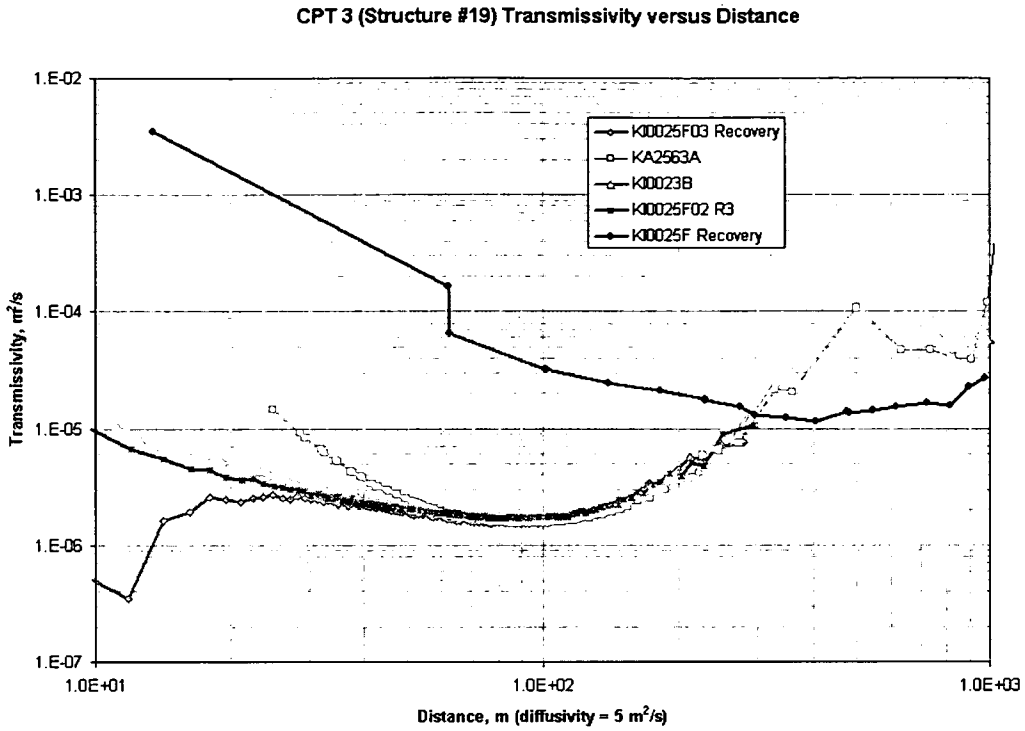

Figure 2-13 Distance-Transmissivity Plot for CPT-3

Evaluation of the derivative provides the following observations:

- The local transmissivity around the pumping well KI0025F03 is low. This may be due to skin effects or local heterogeneity in Structure #19.
- The later time responses are very consistent in monitoring sections of KI0025F02, KI0023B, KA2563.
- A lower derivative, and a higher transmissivity is found near the monitoring section in KI0025F.
- The response shows a partial dimension, which may indicate heterogeneity in the fracture network connected to and comprising Structure #19.

Evaluation of the transmissivity-distance plot (Figure 2-13) provides the following insights:

- The region around the tested section for CPT-3 has similar if heterogeneous properties (local low transmissivity at KI0025F03).

- KA2563A may be near a no-flow boundary.
- KI0025F response indicates the presence of a higher transmissivity region.
- All zones see high transmissivity in late time, possibly the high transmissivity region around KI0025F.
- This high transmissivity region is about 100-200 meters from KI0025F03. This may be the "Z-structure" in the hydrostructural model, or another major bounding feature being constant pressure boundary for Structure #19.

Figure 2-14 shows the comparison between the response see in CPT-3 against the responses seen in the Structure #20 complex during the TRUE-BS project. The responses are in a consistent range and magnitude.

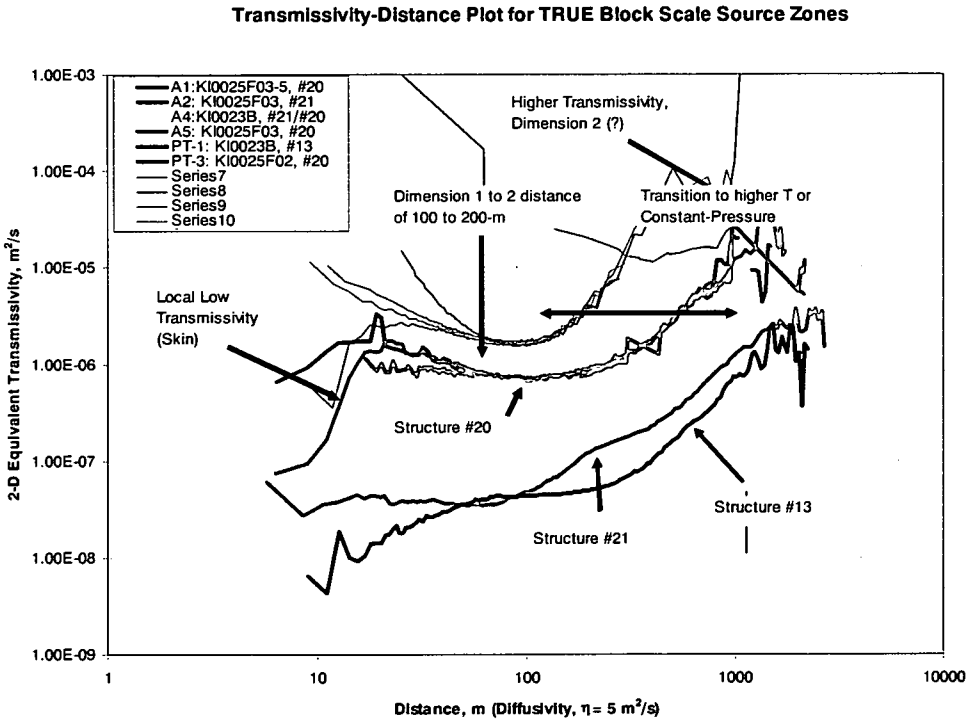

Figure 2-14 Comparison of CPT-3 tests against Structure#20 region responses

The following conclusions were reached regarding the implications of CPT-3 analysis for the Structure #19 region hydrostructural model.

- Structure #19 has consistent behavior with structure #20, about a 5x increase in transmissivity.
- Structure #25 may be a real, lower transmissivity background structure.
- The feature observed to intersect borehole KA2563A is a splay of structure #19, and not an independent structure.
- The structure which intersection KI0025F:R1 is probably the large Z structure. This intersection indicates a low transmissivity structure connected to #19 but also to a major structure which ties in a lower head.
- There is a potential background fracture in KI0025F:R3. This is important because one of the goals of the project is to obtain additional test results for background fracture networks.
- The higher dimension observed at greater distance in structure #19 is a possible effect of intersecting fractures.
- The partial dimension observed in CPT-3 indicates a possible heterogeneous network in Structure #19.

2.2.2 Analysis of Dilution and Tracer Tests

The Discrete Fracture Network (DFN) model we are using is the Task 6C 200-m scale hydrostructural model (Dershowitz et al., 2003; Hermanson and Doe, 2000). Figure 2-15 shows the deterministic and stochastic features of the model.

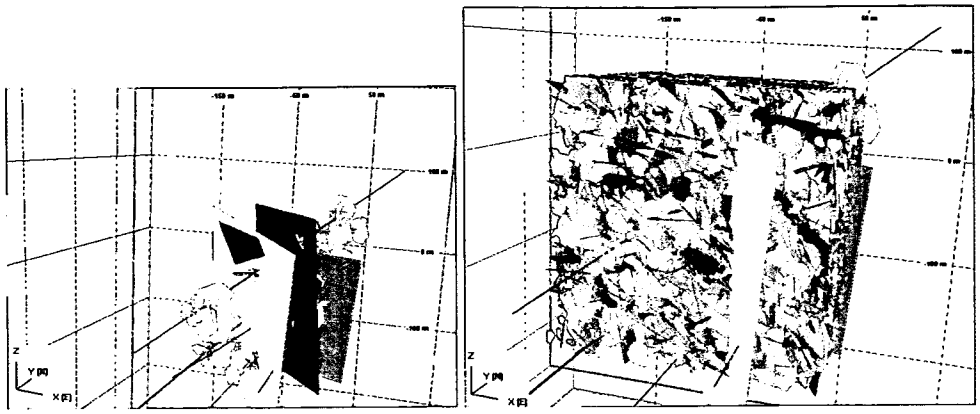

Figure 2-15 TRUE Block scale region DFN model looking northwest. (a) Deterministic features with the larger fractures (>200m) removed for clarity. Structure #19 in orange. (b) Background fractures included

CPT Experiments

For the TRUE-BSC CPT series of experiments, boreholes KI0025F02 and KI0025F03 were re-instrumented to better focus on the desired target, Structure #19 (Figure 2-15). The re-instrumented intervals are labeled "R". For proper simulation, "virtual" packers need to reflect the new experimental configuration and these data are calculated in the spreadsheets:

KI0025F02_Reinstr.XLS, and
KI0025F03_Reinstr.XLS

Packer *intervals* are provided in the data delivery, but this information needs to be converted to packer *coordinates and depths*. To calculate these data the "Secup" value for the section of interest and the "Seclow" value for the adjacent section number are noted. As an example, in the following data set, say the interval is number 9.

Section Number	Start Date	Secup (m)	Seclow (m)	Structure
P10	9/2/03 0:00	3.4	55.1	5,6,7
P9	9/2/03 0:00	56.1	63	23
P8	9/2/03 0:00	64	72.3	22

Thus the data to be entered for "Packer 9" in the SAB calculation spread sheet is:

	55.1	-21.6279	35.5097	-21.8203	1
Pkr9	56.1	-20.7774	35.1967	-22.2429	6.9

Thus "Pkr9" marks the top of section P9. The bottom of Pkr9 is the "Secup" value for P9 (56.1m) and the top of Pkr9 is the base of section P10 (55.1m). These are the proper coordinates and depths needed to create structures in a SAB file.

2.3 Hydraulic Interference Simulations

Golder carried out transient flow simulations for the interference experiments described in the Data Delivery document "BS2B D1_F02short.doc". These simulations were carried out using FracMan/MAFIC, and focused on the re-instrumented R3 section KI0025F02, the pumping well, which intersects Structure #19. The following sections of the observation wells also intersect this structure:

KA2563A_S3 KI0023B_P2 KI0025FO3_R3 KI0025F_S2 KA2511A_T3

The model is developed in stages and assessed based on comparisons of the simulated and measured drawdown curves.

General modeling procedure:

1. Implement the "Task 6C" hydrostructural model, both including background fractures, and without background fractures.
2. Apply 200m-block region hydraulic boundary conditions based on D. Holton simulation for the TRUE-BS project.
3. Simulate to steady state using FracMan/MAFIC.
4. Apply appropriate group flux values at the boundary group representing the R3 section of pumping well KI0025F02. These values are derived from the Data Delivery document "BS2B D1_F02short.doc". Flow is out of the section at rates of 1.78, 1.66, and 1.64 L/minute for a duration of 20 minutes after which the flow lines are closed. These data are converted to m^3/sec.
5. Simulate transient flow using FracMan/MAFIC.

2.3.1 Model Calibration Simulations

First run: The TRUE Block Scale combination of deterministic and background fractures was used to begin the hydraulic interference simulation. The transmissivity of Structure #19 was left at the value for other many of the other structures in the region (1.8E-06 m^2/s). The resultant transient flow solution showed very little match to the field measurements (Figure 2-16). For instance, there is only a negligible response at the observation wells and just ~5 meters of drawdown at the pumping section (KI0025F02:R3) where field measurements showed nominally 200 meters of drawdown.

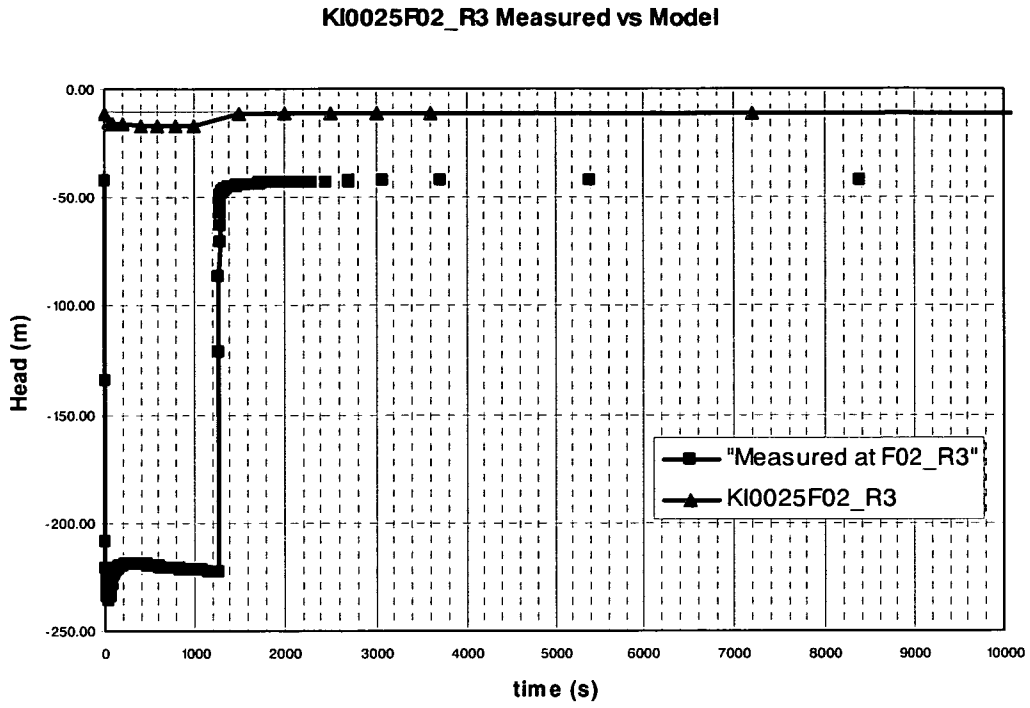

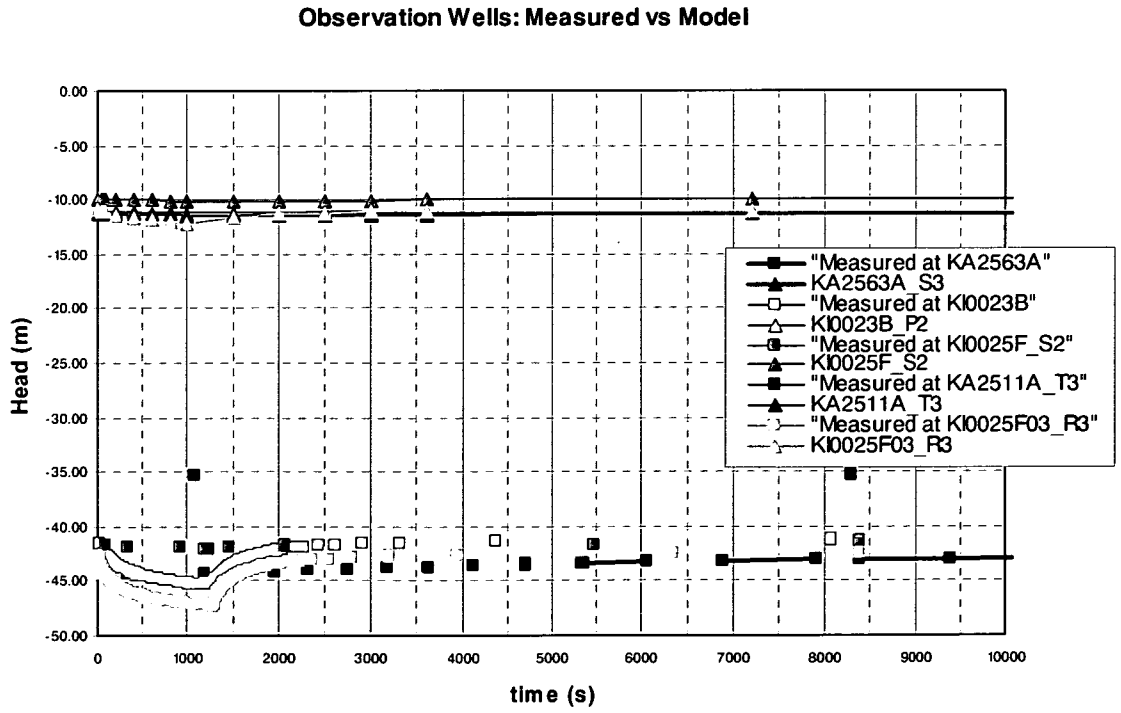

Figure 2-16 Comparison of measured and modeled drawdown curve for the TRUE Block scale region. (b) Modeled drawdown curves for observation sections in the region

Second run: The first adjustment to the model was to remove the background fractures from the simulation. Steady-sate and transient flow solutions were recalculated using the newly constructed mesh geometry. Removal of the background fractures results in noticeable responses in all of the observation wells. For instance the drawdown is effectively doubled at the R3 section of the nearby KI0025F03 observation well (from a nominal 1 meter to 2 meters,) and doubled at pumping section R3 of well KI0025F02 from roughly 6 meters to 12 meters (see Figure 2-17).

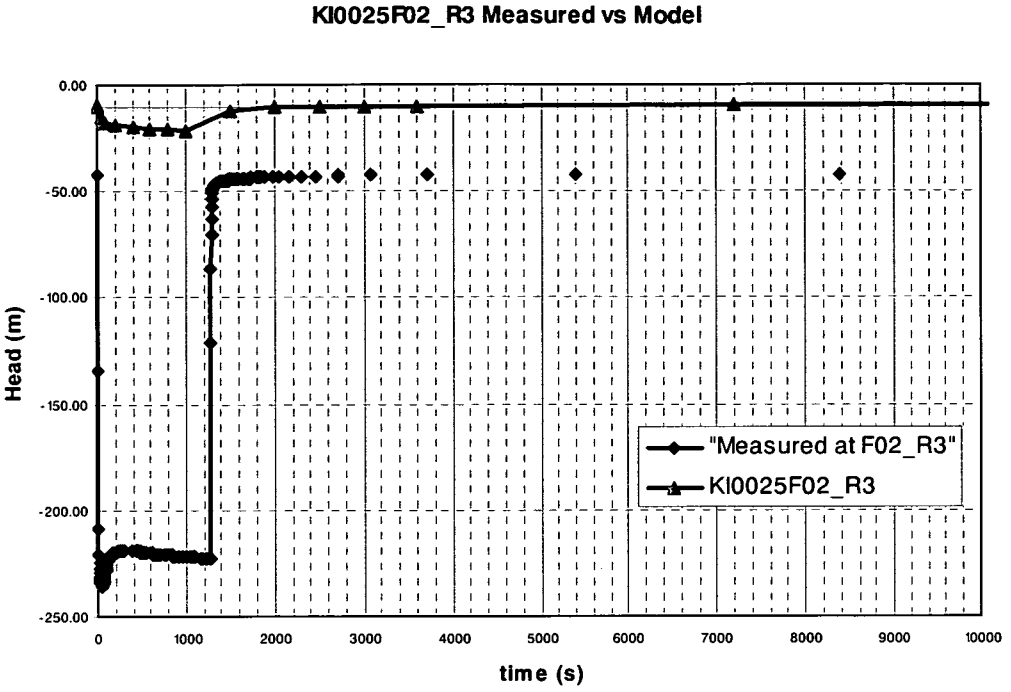

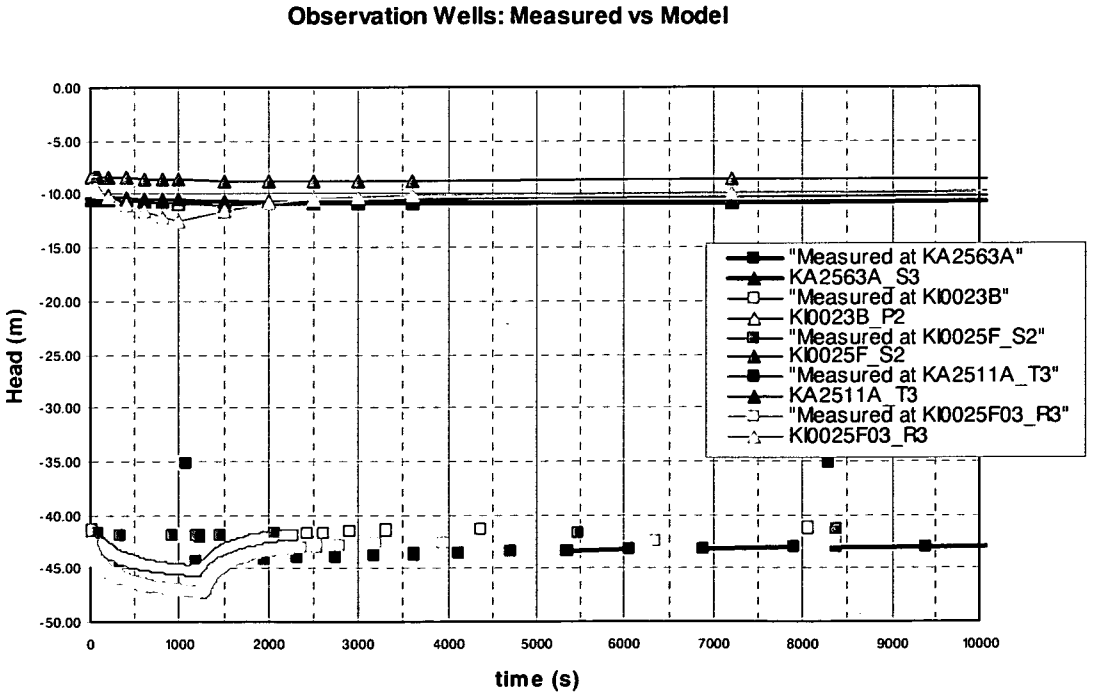

Figure 2-17 Comparison of measured and modeled drawdown curves. Model removes effect of background fractures from the TRUE Block scale region. (b) Modeled drawdown curves for observation sections in the region

Third run: The second adjustment to the hydraulic interference model was to lower the transmissivity of Structure #19. Conceptually, this could limit the flow at KI0025F03 greatly enhancing the drawdown during pumping. For the previous simulations the transmissivity value for used for Structure #19 was that of many of the other structures in the True Block Scale 200 meter region (1.8E-06 m^2/sec). A previous technical report lists transmissivity values for deterministic structures in the study region. The value listed for Structure #19 is an order of magnitude lower at 1.1E-07 m^2/sec (see "Final Report of the TRUE Block Scale project TR-02-13 part 1" (April 2002), Table 4-15 p. 120). Thus for the new simulation, transmissivity values were changed to 1.1E-07 at mesh geometry nodes representing Structure #19. Once again new steady state and transient flow solutions were calculated. The results now show good agreement between the amount of measured and simulated drawdown at all the observing well sections. For instance, at KI0025F03 section R3, the simulated drawdown is now close to 3 meters, which compares to the measured value of roughly 4 meters (see Figure 2-18). However while there is also an enhancement of the simulated drawdown at the pumping well to ~16 meters, this is still nowhere near the measured value of ~200 meters.

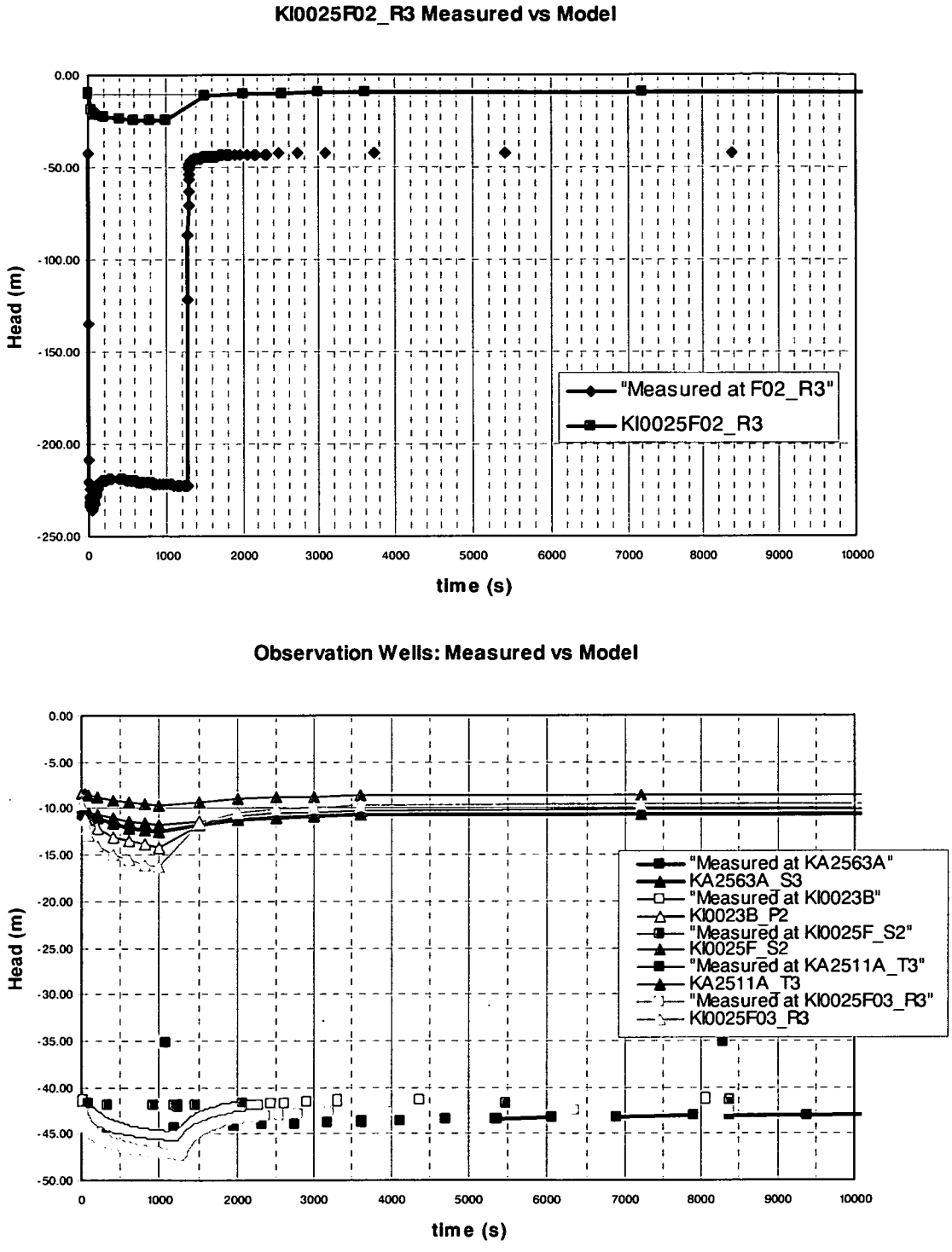

Figure 2-18 Comparison of measured and modeled drawdown curves. Model includes a transmissivity of 1.1E-07 m^2/sec for Structure #19. (b) Modeled drawdown curves for observation sections in the region

Fourth run: The third and final adjustment to the hydraulic interference model was to simulate a "skin effect" of low transmissivity drilling material around the pumping well. The idea is to account for the high degree of measured drawdown in the pumping section yet cause no additional effects on the simulation results at the observation wells.

In order to set up the new simulation, a new "mixed" mesh geometry was calculated for the region. This new solution has finer meshes on the 2.5-meter scale in the vicinity of boreholes and regular "coarse" meshes on the 10-meter scale over the breadth of the study region.

During the mesh calculation a radius of 3 meters was used to define a "cylinder" around section R3 of pumping well KI0025F02. Then using the edmesh program, a skin effect could be modeled by simply lowering the effective transmissivities of all the mesh geometry nodes within this cylinder. A transmissivity value of 2E-08 m^2/sec was used. To complete the simulation, steady-sate and transient flow solutions were recalculated using this new "mixed mesh" geometry.

The results show that modeling a skin effect around KI0025F02:R3 greatly increases its drawdown yet preserves the good match of simulated and measured drawdowns at the observation wells (Figure 2-19). The simulated drawdown at the pumping well is now about 190 meters which compares to the measured value of ~200 meters.

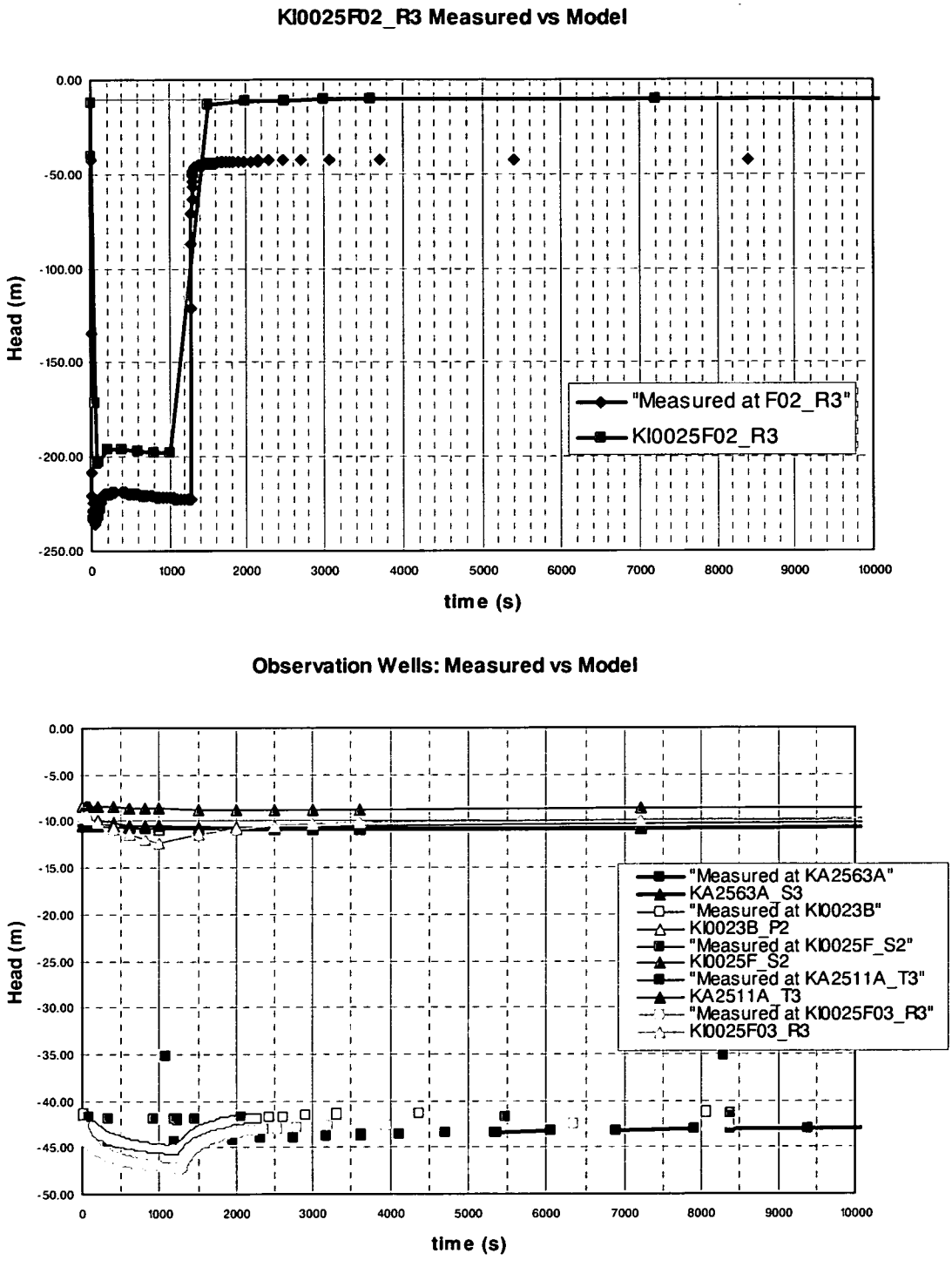

Figure 2-19 Comparison of measured and modeled drawdown curves. Model includes a "skin effect" around pumping well KI0025F02:R3. (b) Modeled drawdown curves for observation sections in the region

The fluid pathways in these test scenarios are all within Structure #19 and run from the pumping well section (KI0025F02:R3) to the observation well section. A general, positive correlation of pathway distance and maximum drawdown can be seen (Table 2-7). It should be noted that while the simulated absolute head values are offset from the absolute head measurements, the accuracy of the present hydro-structural model is best judged by comparing *relative* measured and simulated drawdown as we have done. At any location in the hydro-structural model, the head value can be scaled to match that of the field measurements but this has no effect on the simulation analysis.

In summary the hydraulic interference simulations yield a hydro-structural model with the following salient features:

- No background fractures.
- A lower transmissivity for Structure #19 equal to 1.1E-07 m^2/s.
- A simulated skin effect around section KI0025F02:R3.

Table 2-7 Pathway distances from pumping well KI0025F02:R3 to the observation sections, maximum drawdown for the hydraulic interference model simulation, and measured maximum drawdown

Section	Distance (m)	Simulated Max. Drawdown (m)	Measured Max. Drawdown (m)
KI0025F03:R2	--	186	193
KI0025F03:R3	19	2.8	4.0
KI0023B:P2	38	1.0	3.2
KI0025F:R2	50	0.2	0.5
KA2563A:S3	70	0.1	1.5
KA2511A:T3	92	0.2	~0

2.3.2 Hypothesis Testing

On behalf of JNC, Golder worked with Anders Winberg of SKB to develop the hypotheses to be tested in the TRUE-Block Scale Continuation Project (TRUE-BSC). These hypotheses for the BS2B phase of TRUE-BSC are in two general groups related to (I) the nature of transport in fracture networks in general, and (II) transport in background fractures in particular:

- Hypothesis Ia) Microstructural information can provide significant support for predicting retention at experimental time scales
- Hypothesis Ib) transport at experimental time scales is significantly different for faults and joints, due to the microstructural differences between them
- Hypothesis Ic) longer distance pathways are dominated by fault fracture behaviour, while shorter pathways can be dominated by joint fracture behaviour.
- Hypothesis IIa) transport pathway branching can be demonstrated to occur in networks of background fractures
- Hypothesis IIb) mixing at fracture intersection can be demonstrated to occur in networks of background fractures.
- Hypothesis IIc) fracture retention properties tend to be scale dependent primarily due to difference in microstructure.

In situ tests and modelling of longer flow paths in single intermediate sized structures is intimately connected to understanding better transport of radionuclides from the close proximity network around a canister position to, and within an intermediate fracture zone. Integration of available TRUE Block Scale (and Äspö) information and data for model prediction and performance of a test in such a structure could be a valuable contribution to understanding flow and transport in crystalline rock.

To test the above hypothesis, B2B will use geologic data to interpret retention properties. That is, given the fracture mineralogy, a spatial distribution of porosity, the geometry and properties of gouge and other structural details, can one evaluate retention realistically? If so, then site selection and characterization programs that are in their early stages can use a geologic description from core to estimate retention properties long before tracers can be introduced. These evaluations can be very valuable ranking and assessing candidate locations.

Injection in (low-transmissive) background fractures connecting to fracture/structure networks is a valuable contribution to understanding the other extreme, i.e. conductive elements which are likely to be connection to, or being located in the close vicinity of a canister position. The key

issues here are pathway branching and mixing at fracture intersections. We will strive to identify background fracture pathways which can be used to characterize and test these processes.

2.4 Solute Transport Simulations

The CPT-1 through CPT-3 experiments were run as tracer dilution rather than tracer test simulations. However, for the present purposes, PAWorks was used to run the CPT-1 through CPT-3 experiments as if they had been conventional tracer experiments, for comparison based on breakthrough curves rather than tracer dilution curves. Simulations will be carried out for the actual tracer dilution experiments over the next few weeks.

The tracer test simulations were carried out using the DFN model calibrated to the hydraulic interference results from this study.

The CPT-4 tracer test was simulated based on information provided in the SKB Data Delivery document "Status_Report_CPT1-3_2003-10-20_PtA.doc".

The simulations of the CPT-1, 2, and 3 experiments assumed non-sorbing tracer transport (^{186}Re), with injection of a decaying-pulse type (Figure 2-20).

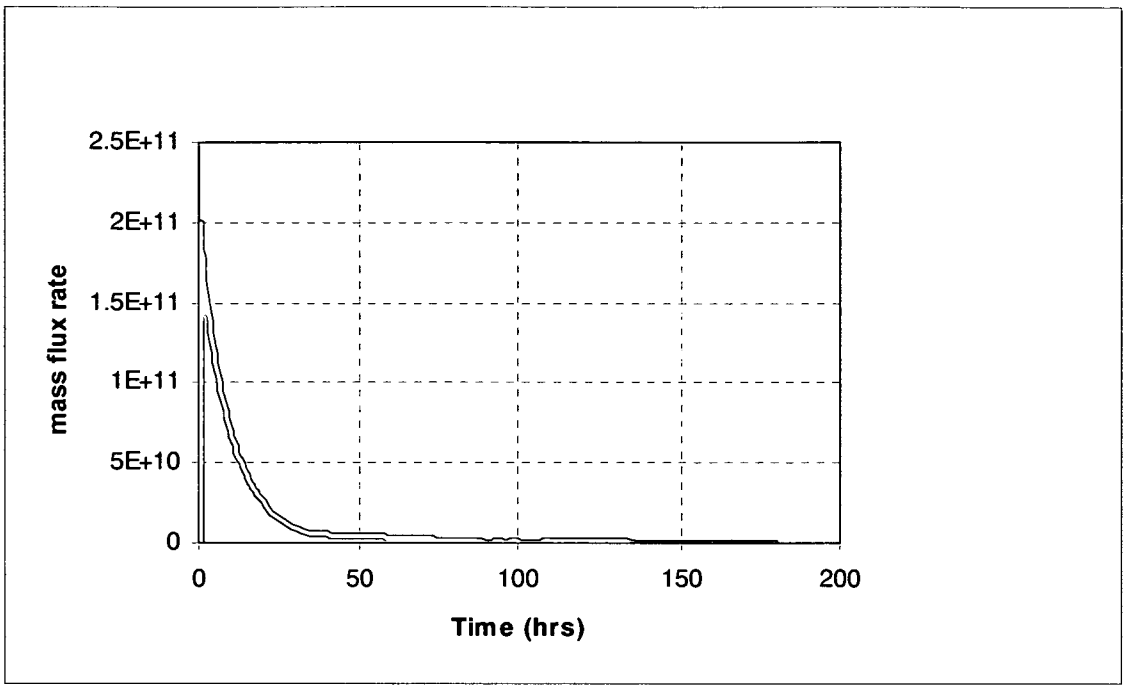

Figure 2-20 Injection curve used in CPT-1, 2, and 3 tracer test simulations

PAWorks was used to determine a transport solution, i.e., sets of nuclide pathways through the region given the parameters for the hydro-structural model. The pathway results were then supplied to the LTG (Laplace Transform Galerkin) program, which calculates the recovery of tracer material at the desired areas in the study region. The results of simulation of CPT-1, 2, and 3 transport pathways are shown in Figure 2-21 through Figure 2-26 and Table 2-8 through Table 2-13.

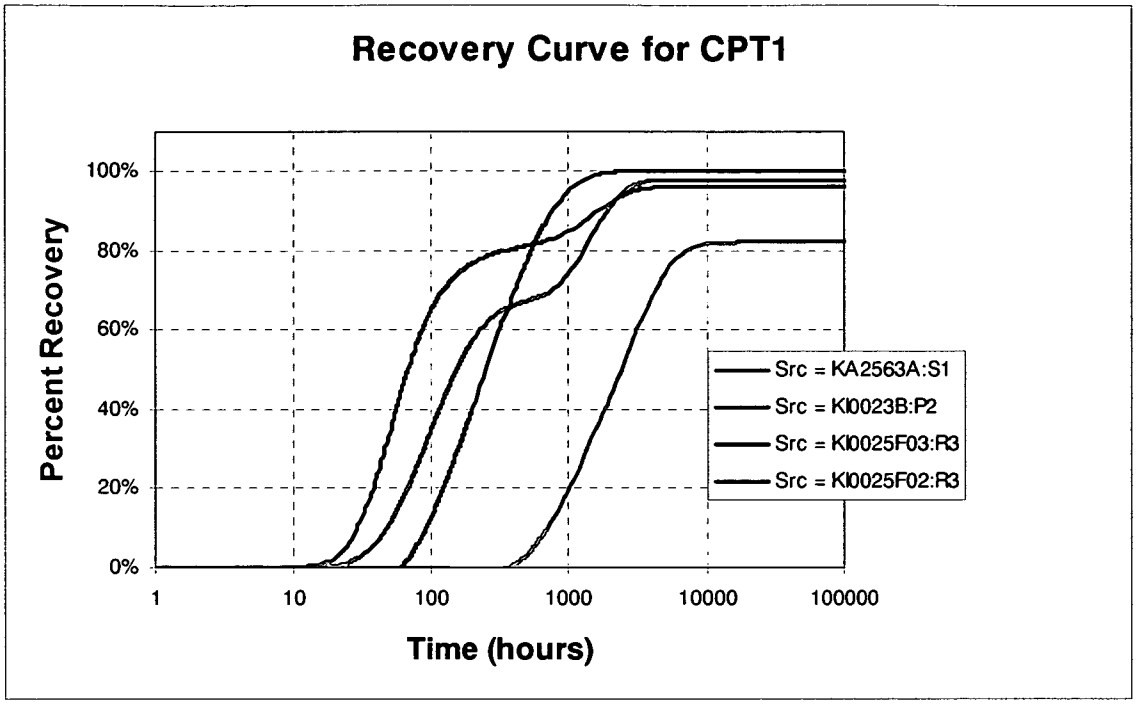

Figure 2-21 Predicted cumulative recovery curves for Rhenium, test CPT-1

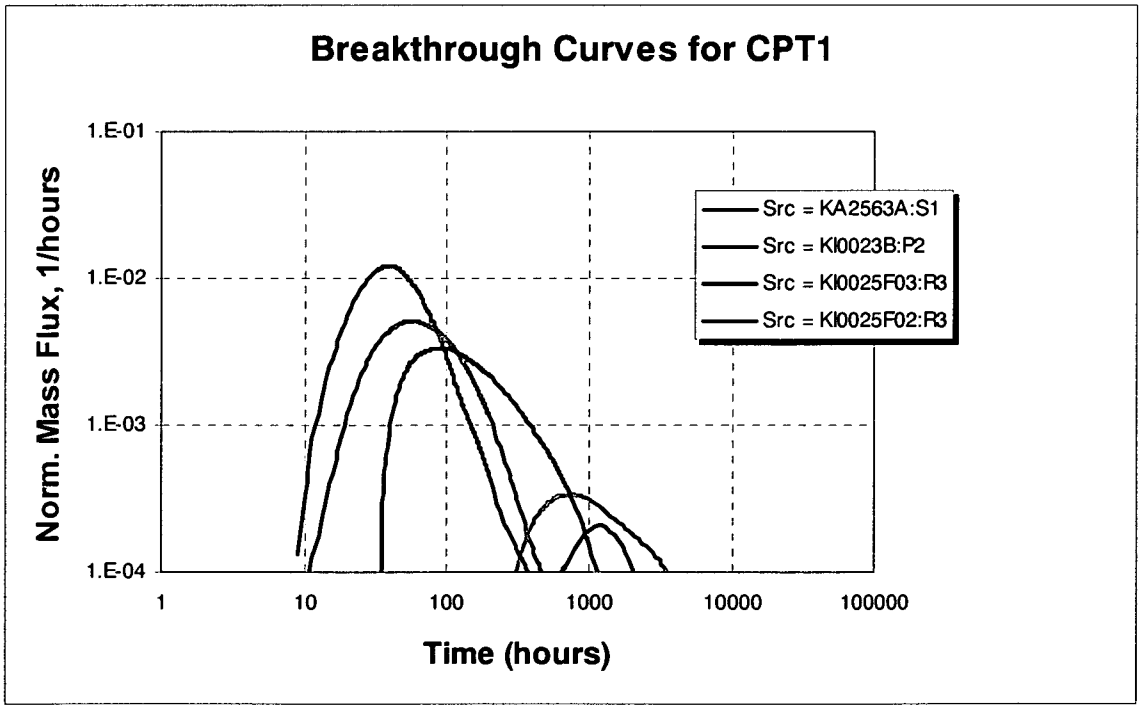

Figure 2-22 Predicted breakthrough curves for Rhenium, test CPT-1

Table 2-8 Predicted characteristic times (in hours) and total recovery at 10,000 hours for test CPT-1 (sink = KI0025F:R2)

Metric	KI0025F02:R3	KI0025F03:R3	KI0023B:P2	KA2563A:S1
T_5	77.0	23.5	36.5	565.0
T_{50}	250.0	68.0	155.2	2420.0
T_{95}	1048.5	299.8	2603.5	N/A
@10K Hrs	100.0%	96.1%	97.6%	82.0%

Table 2-9 Predicted change in flux (ΔQ, ml/hr) compared to measured values for test CPT-1 (sink = KI0025F:R2)

Metric	KI0025F02:R3	KI0025F03:R3	KI0023B:P2	KA2563A:S1
T_5	+24.7	+51.4	+15.2	+2.6
T_{50}	+13.2	+43.8	+7.2	+1.3
T_{95}	+1.2	+1.3	<1	N/A
Measured	-2	+58	+4	-5

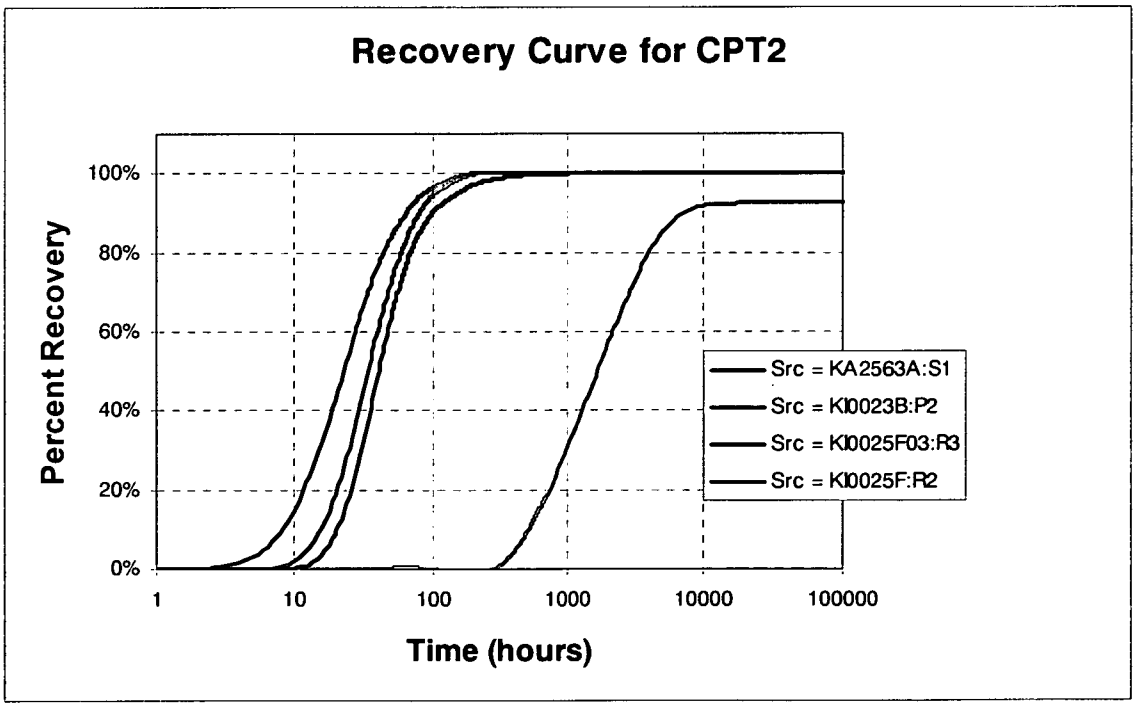

Figure 2-23 Predicted cumulative recovery curves for Rhenium, test CPT-2

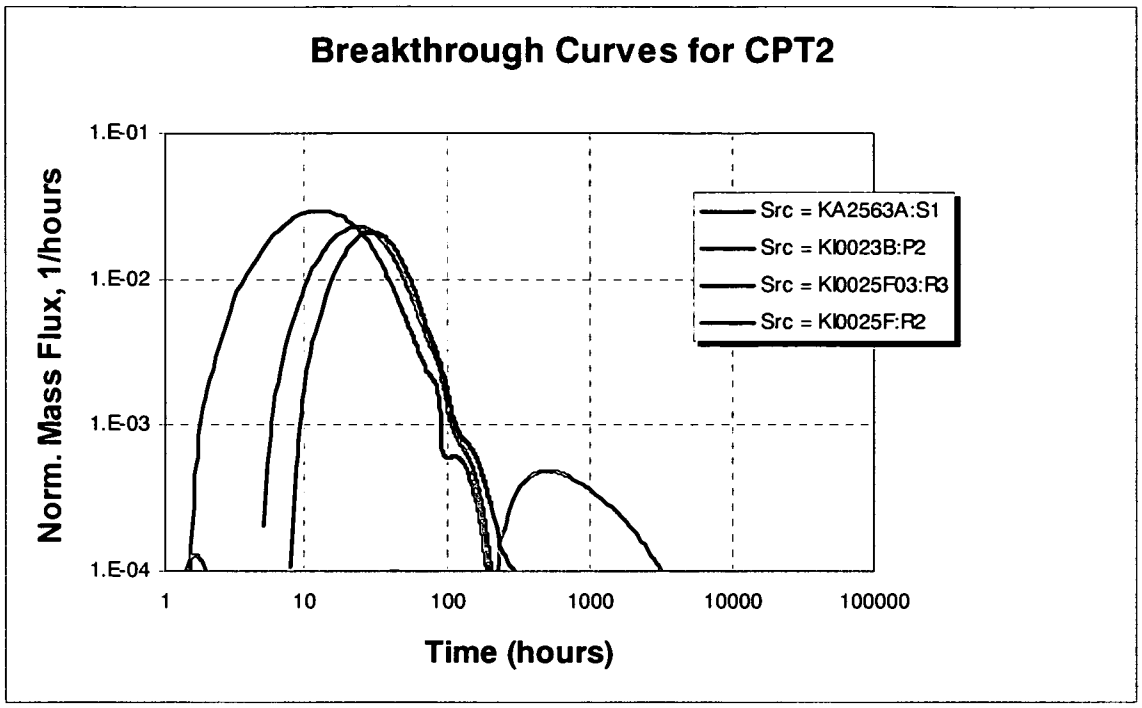

Figure 2-24 Predicted breakthrough curves for Rhenium, test CPT-2

Table 2-10 Predicted characteristic times (in hours) and total recovery at 10,000 hours for test CPT-2 (sink = KI0025F02:R3)

Metric	KI0025F:R2	KI0025F03:R3	KI0023B:P2	KA2563A:S1
T_5	17.2	6.5	12.7	410.2
T_{50}	41.0	23.0	34.1	1650.0
T_{95}	154.3	86.9	104.3	N/A
@10K Hr	100.0%	100.0%	100.0%	91.9%

Table 2-11 Predicted change in flux (ΔQ, ml/hr) compared to measured values for test CPT-2 (sink = KI0025F02:R3)

Metric	KI0025F:R2	KI0025F03:R3	KI0023B:P2	KA2563A:S1
T_5	+86.5	+1.3	+47.1	+4.1
T_{50}	+122.0	+139.5	+71.0	+2.1
T_{95}	+4.6	+10.8	+4.0	N/A
Measured	+47	+420	+10	+9

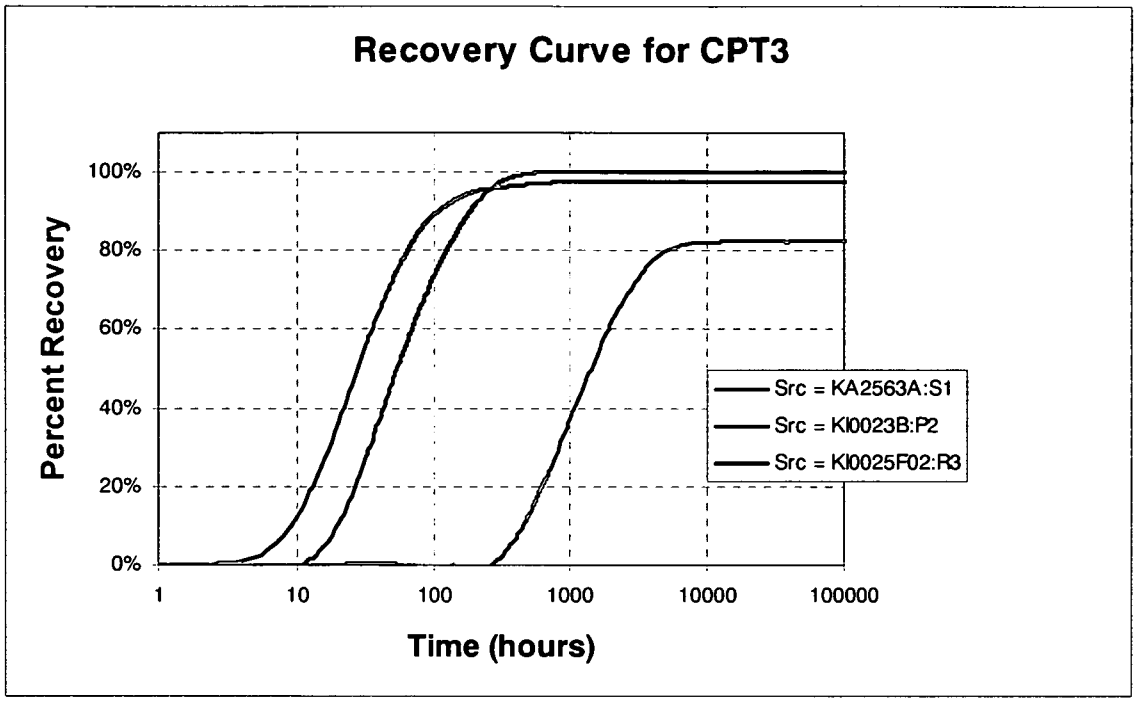

Figure 2-25 Predicted cumulative recovery curves for Rhenium, test CPT-3

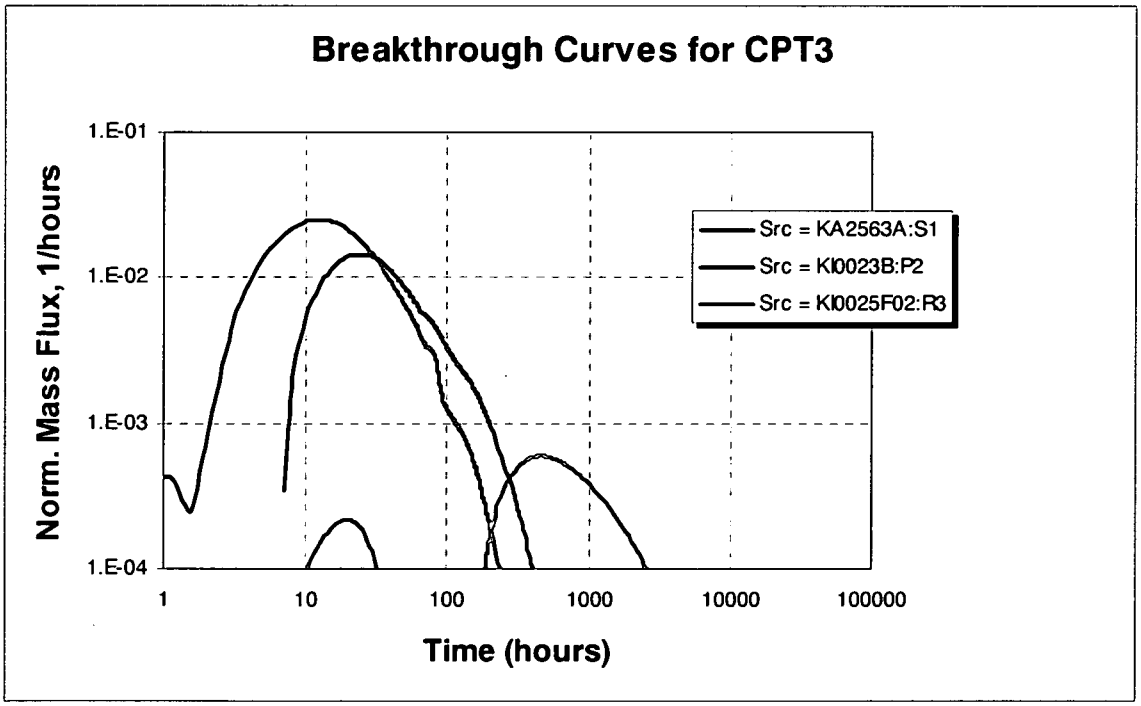

Figure 2-26 Predicted breakthrough curves for Rhenium, test CPT-3

Table 2-12 Predicted characteristic times (in hours) and total recovery at 10,000 hours for test CPT-3 (sink = KI0025F03:R3)

Metric	KI0025F02:R3	KI0023B:P2	KA2563A:S1
T_5	16.5	6.7	365
T_{50}	54.9	27.9	1415
T_{95}	249.8	198.2	N/A
@10K Hrs	100.0%	97.5%	82.3%

Table 2-13 Predicted change in flux (ΔQ, ml/hr) compared to measured values for test CPT-3 (sink = KI0025F03:R3)

Metric	KI0025F02:R3	KI0023B:P2	KA2563A:S1
T_5	+92.9	+62.3	+4.4
T_{50}	+57.8	+55.0	+2.2
T_{95}	+4.0	<1	N/A
Measured	+58	+13	+23

2.4.1 Reporting

During H-15, Golder supported JNC with the following reporting activities for the TRUE-BSC project.

Preparation of the experimental design document,

> Winberg, A., B. Dershowitz, P. Anderson, and T. Doe, 2003. TRUE Block Scale Continuation Technical Memorandum. Results of BS2A feasibility odeling and recommendations for priorities for BS2B in situ tests. SKB, April.

Completion of the TRUE-BS project reports,

> Dershowitz, W., K. Klise, A. Fox, S. Takeuchi, M. Uchida, 2003. Channel network and discrete fracture network analysis of hydraulic interference and transport experiments and prediction of Phase C experiments Swedish Nuclear Fuel and Waste Management Company (SKB), Äspö Hard Rock Laboratory, Progress Report IPR-29-02. SKB, Stockholm

Dershowitz, W., and K. Klise, 2003. Evaluation of fracture network transport pathways and processes using the Channel Network approach. Swedish Nuclear Fuel and Waste Management Company (SKB), Äspö Hard Rock Laboratory, Progress Report IPR-02-34. SKB, Stockholm

Winberg A., P. Andersson, Byegård, J., A. Poteri, V. Cvetkovic., W. Dershowitz, T. Doe, J. Hermanson, J. Gómez-Hernández, A. Hautojärvi, D. Billaux, E.-L. Tullborg, D. Holton, P. Meier, and A. Medina, 2003. Final report of the TRUE Block Scale project. Swedish Nuclear Fuel and Waste Management Company (SKB), Äspö Hard Rock Laboratory, Technical Report TR-02-16. SKB, Stockholm.

3. TASK 2: MIU PROJECT DISCRETE FRACTURE ANALYSIS

During H-15, Golder assisted JNC in interpretation of hydraulic experiments carried out at the MIU Site. This effort was carried out through three subtasks:

- Task 2.1: MIU Hydraulic Test Interpretation
- Task 2.2: MIU Hydrostructural Synthesis
- Task 2.3: MIU DFN Modeling

3.1 Task 2.1: MIU Hydraulic Test Interpretation

During HY-15, Golder Associates assisted JNC/Tono in the analysis and review of MSB shallow borehole hydraulic tests, and the MIZ-1 borehole dynamic data.

3.1.1 Site Visit

During the week of September 8th, 2003, Golder Associates hydrogeologist Christian Enachescu visited S. Takeuchi and his colleagues at JNC/Tono. At JNC/Tono, Christian carried out of a review of MSB shallow borehole and MIZ-1 deep hydraulic tests.

3.1.2 Evaluation of MSB Tests

The evaluated MSB tests are summarized in Table 3-1. For each test, Golder evaluated:

- well installation
- testing geometry
- testing boundary conditions

These tests are analyzed using FlowDim and INTERPRET2 techniques. Figure 3-1 through Figure 3-3 illustrate transmissivity vs. distance interpretative plots for these tests.

The effective transmissivity from the test is provided in the Y axis. The hydraulic distance is provided in the inclined axis. A hydraulic distance of 100 m is marked for reference.

Table 3-1 Analyzed MSB Tests

Test ID	Test Phase	Type of Test
MSB1T1	SI1	head
MSB1T1	SIS1	flux
MSB1T1	SI2	head
MSB1T1	SIS2	flux
MSB3T2	SWS	flux
MSB3T2	PW2	head
MSB3T2	SW	head
MSB4T2	PI1	head
MSB4T2	PI2	head
MSB4T2	SI1	head
MSB4T2	SIS1	flux
MSB4T2	PSR	flux

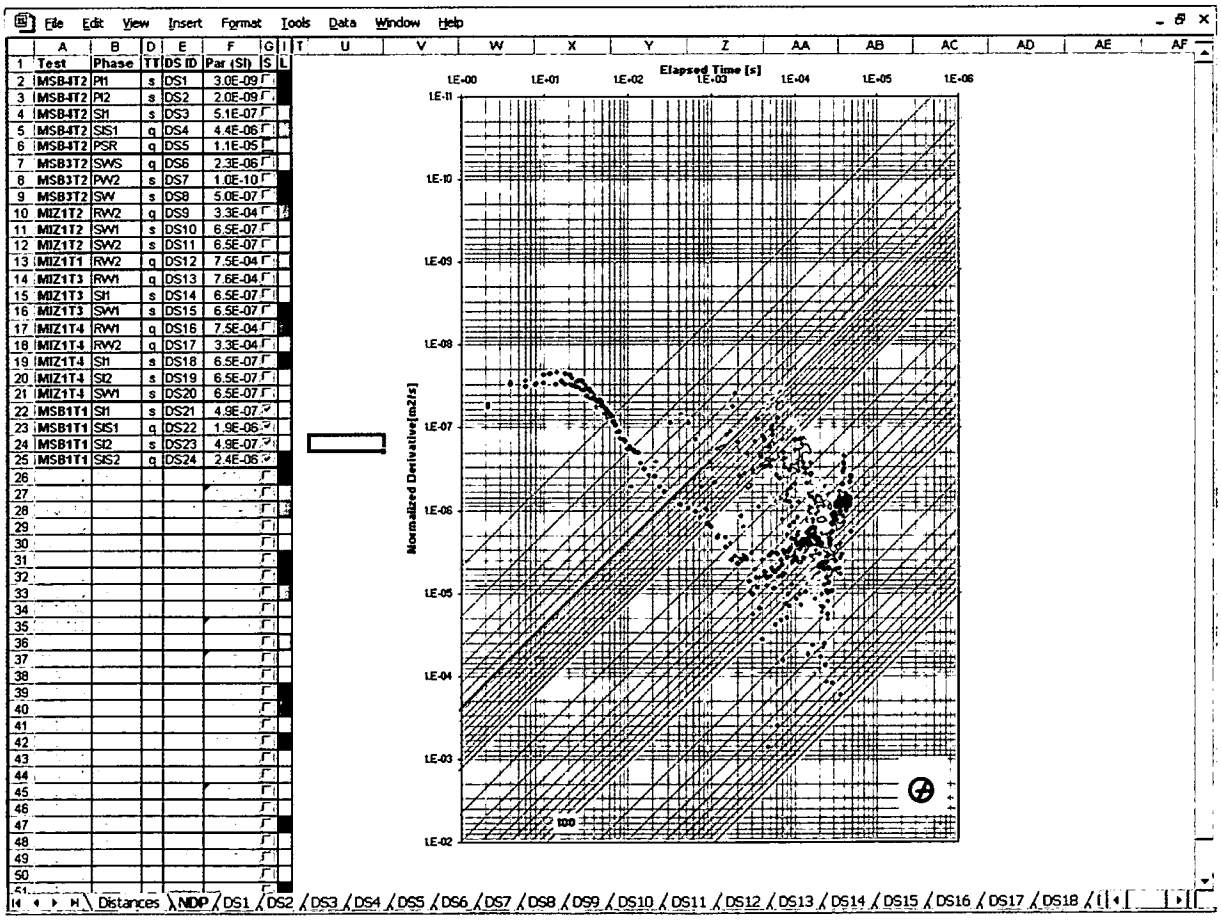

Figure 3-1 MSB-1:T1 Hydraulic Test Interpretations

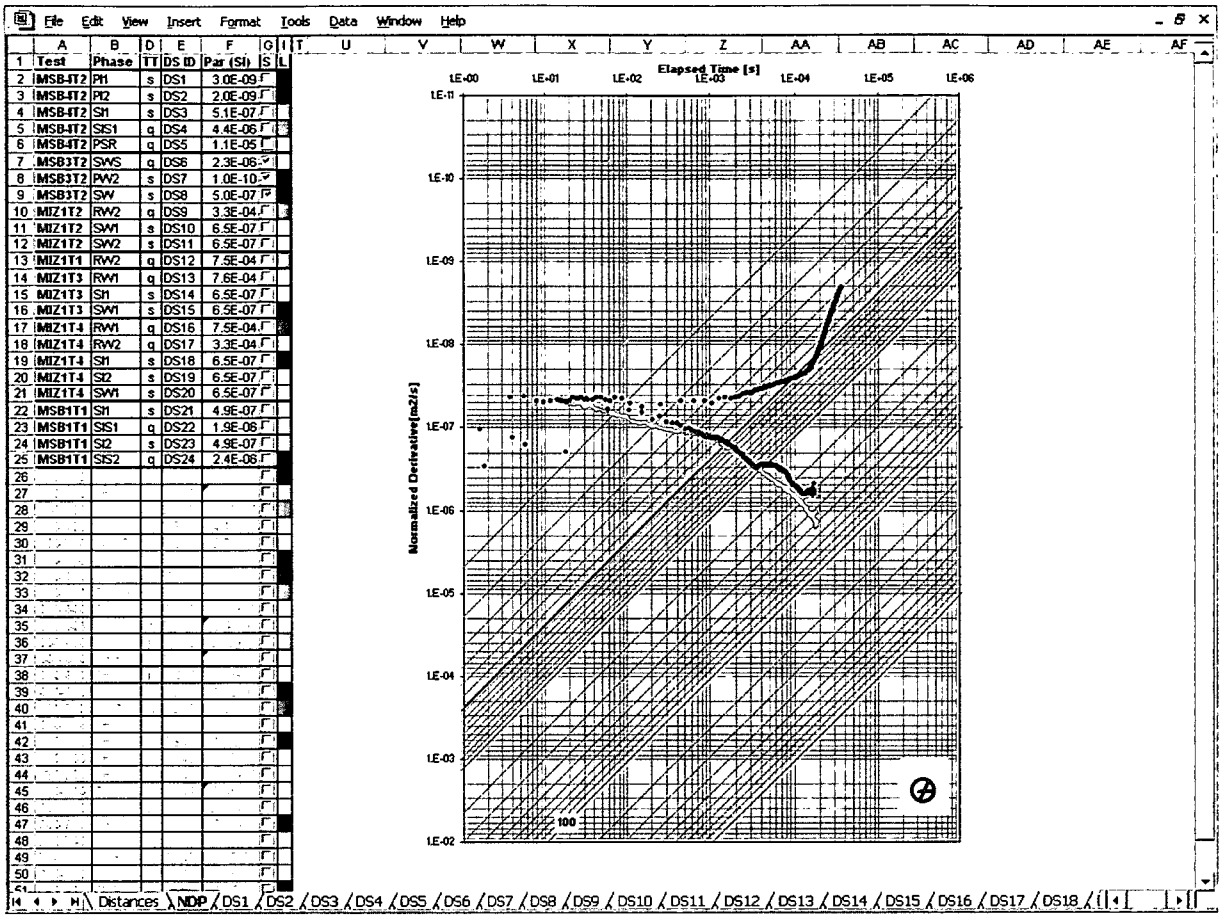

	Test	Phase	TT	DS ID	Par (SI)
2	MSB-IT2	PI1	s	DS1	3.0E-09
3	MSB-IT2	PI2	s	DS2	2.0E-09
4	MSB-IT2	SI1	s	DS3	5.1E-07
5	MSB-IT2	SIS1	q	DS4	4.4E-06
6	MSB-IT2	PSR	q	DS5	1.1E-05
7	MSB3T2	SWS	q	DS6	2.3E-06
8	MSB3T2	PW2	s	DS7	1.0E-10
9	MSB3T2	SW	s	DS8	5.0E-07
10	MIZ1T2	RW2	q	DS9	3.3E-04
11	MIZ1T2	SW1	s	DS10	6.5E-07
12	MIZ1T2	SW2	s	DS11	6.5E-07
13	MIZ1T1	RW2	q	DS12	7.5E-04
14	MIZ1T3	RW1	q	DS13	7.6E-04
15	MIZ1T3	SI1	s	DS14	6.5E-07
16	MIZ1T3	SW1	s	DS15	6.5E-07
17	MIZ1T4	RW1	q	DS16	7.5E-04
18	MIZ1T4	RW2	q	DS17	3.3E-04
19	MIZ1T4	SI1	s	DS18	6.5E-07
20	MIZ1T4	SI2	s	DS19	6.5E-07
21	MIZ1T4	SW1	s	DS20	6.5E-07
22	MSB1T1	SI1	s	DS21	4.9E-07
23	MSB1T1	SIS1	q	DS22	1.9E-06
24	MSB1T1	SI2	s	DS23	4.9E-07
25	MSB1T1	SIS2	q	DS24	2.4E-06

Figure 3-2 MSB-3:T2 Hydraulic Test Interpretations

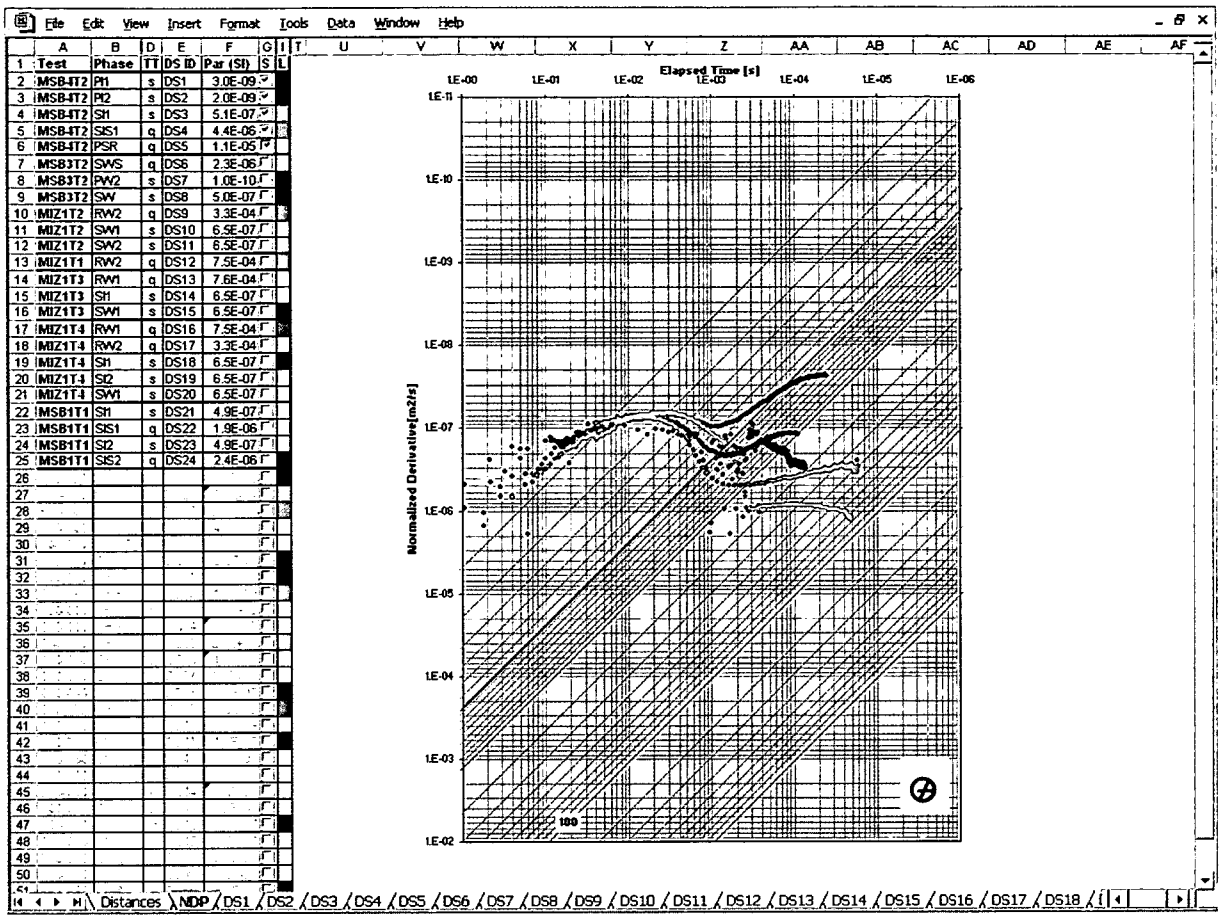

	Test	Phase	TT	DS ID	Par (St)	S
2	MSB-4T2	Pt1	s	DS1	3.0E-09	
3	MSB-4T2	Pt2	s	DS2	2.0E-09	
4	MSB-4T2	St1	s	DS3	5.1E-07	
5	MSB-4T2	SIS1	q	DS4	4.4E-06	
6	MSB-4T2	PSR	q	DS5	1.1E-05	
7	MSB3T2	SWS	q	DS6	2.3E-06	
8	MSB3T2	PW2	s	DS7	1.0E-10	
9	MSB3T2	SW	s	DS8	5.0E-07	
10	MIZ1T2	RW2	q	DS9	3.3E-04	
11	MIZ1T2	SW1	s	DS10	6.5E-07	
12	MIZ1T2	SW2	s	DS11	6.5E-07	
13	MIZ1T1	RW2	q	DS12	7.5E-04	
14	MIZ1T3	RW1	q	DS13	7.6E-04	
15	MIZ1T3	St1	s	DS14	6.5E-07	
16	MIZ1T3	SW1	s	DS15	6.5E-07	
17	MIZ1T4	RW1	q	DS16	7.5E-04	
18	MIZ1T4	RW2	q	DS17	3.3E-04	
19	MIZ1T4	St1	s	DS18	6.5E-07	
20	MIZ1T4	St2	s	DS19	6.5E-07	
21	MIZ1T4	SW1	s	DS20	6.5E-07	
22	MSB1T1	St1	s	DS21	4.9E-07	
23	MSB1T1	SIS1	q	DS22	1.9E-06	
24	MSB1T1	St2	s	DS23	4.9E-07	
25	MSB1T1	SIS2	q	DS24	2.4E-06	

Figure 3-3 MSB-4:T2 Hydraulic Test Interpretations

3.1.3 Evaluation of MIZ-1 Tests

The analyzed MIZ-1 tests are summarized in Table 3-2. These tests were analyzed using the same approaches used for the MSB tests. Transmissivity vs. hydraulic distance plots are provided in Figure 3-4 through Figure 3-7.

Table 3-2 Evaluation of MIZ-1 Tests

Test ID	Test Phase	Type of Test
MIZ1T1	RW2	flux
MIZ1T2	RW2	flux
MIZ1T2	SW1	head
MIZ1T2	SW2	head
MIZ1T3	RW1	flux
MIZ1T3	SI1	head
MIZ1T3	SW1	head
MIZ1T4	RW1	flux
MIZ1T4	RW2	flux
MIZ1T4	SI1	head
MIZ1T4	SI2	head
MIZ1T4	SW1	head

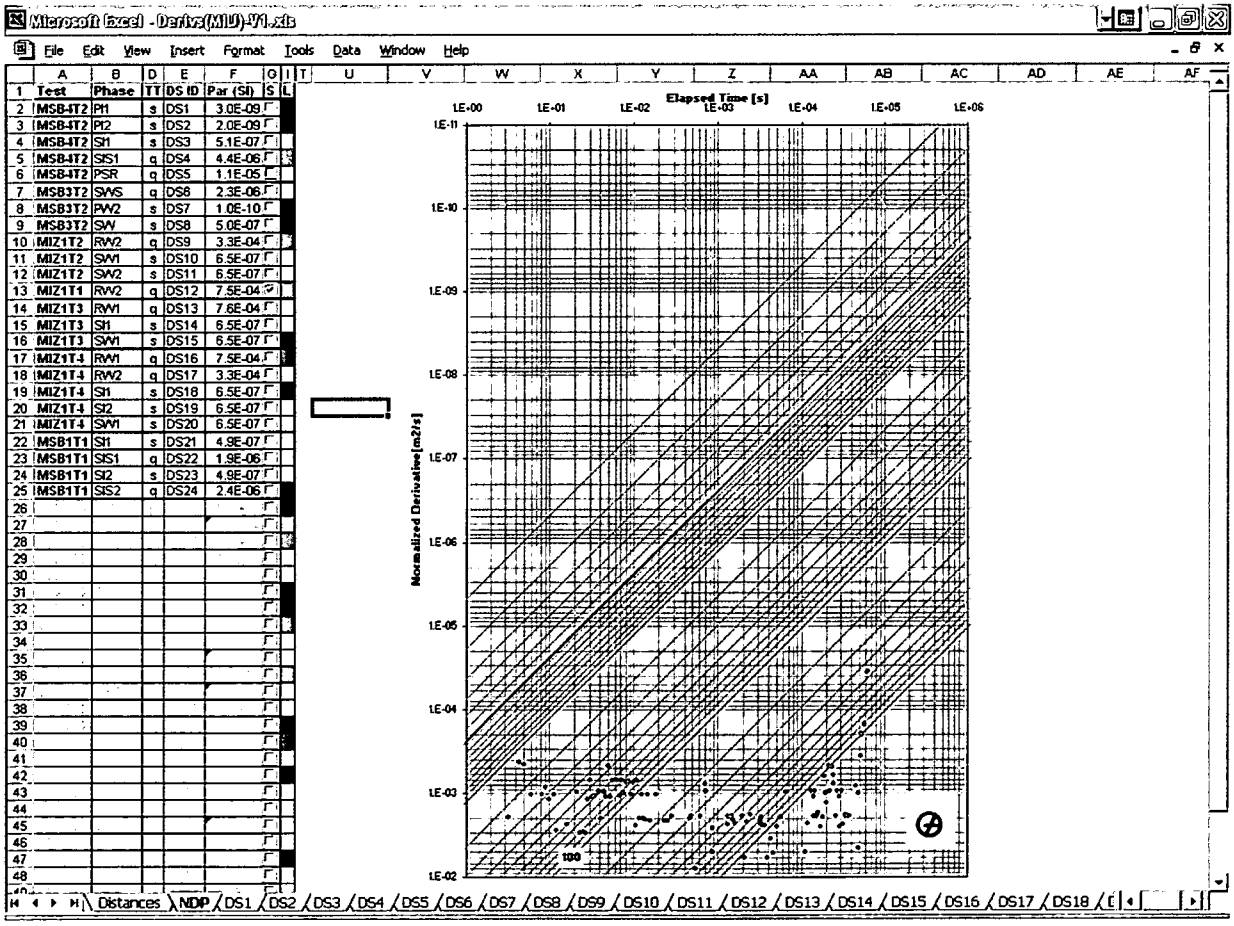

Figure 3-4 MIZ-1:T1 Hydraulic Test Interpretation

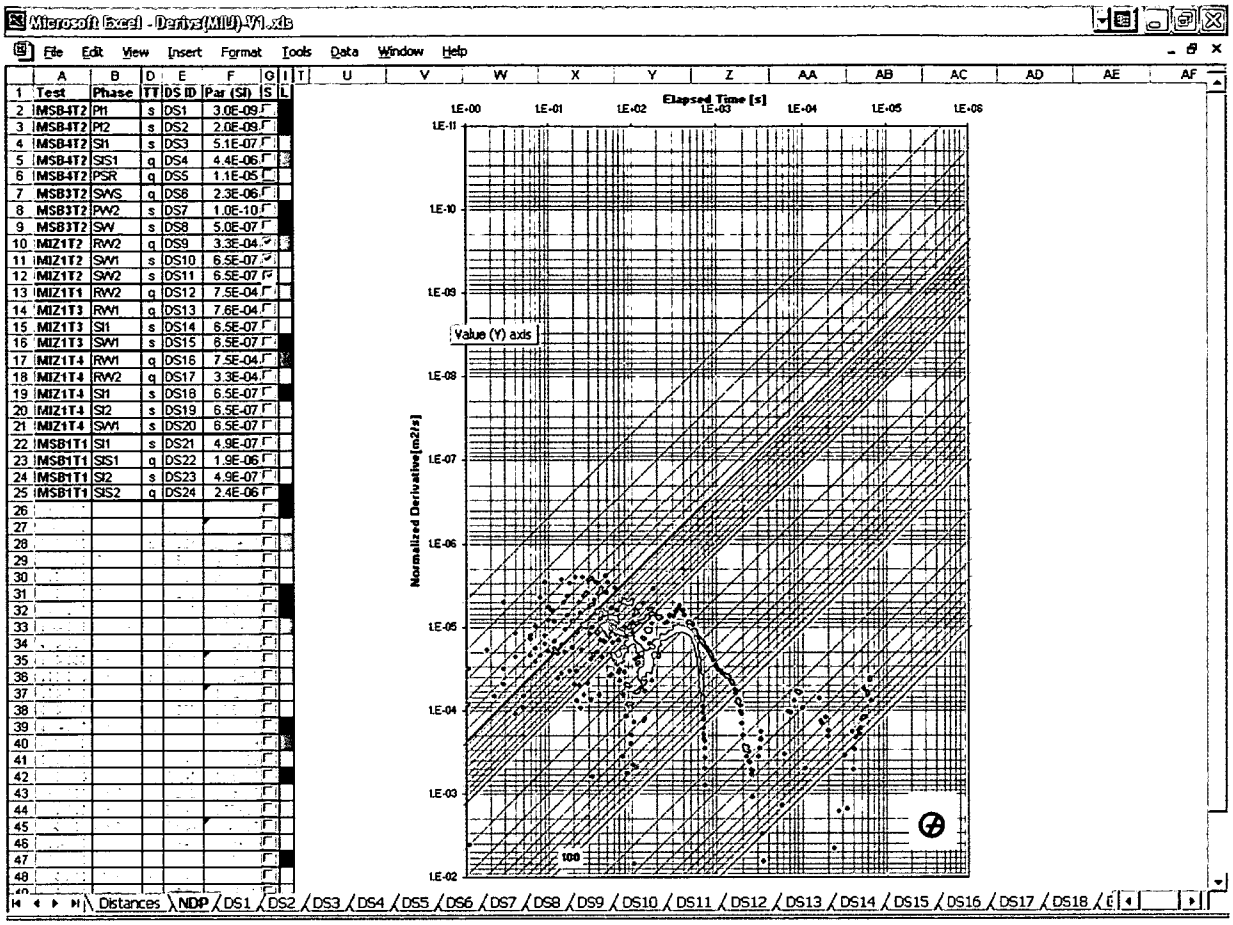

Figure 3-5 MIZ-1:T2 Hydraulic Test Interpretation

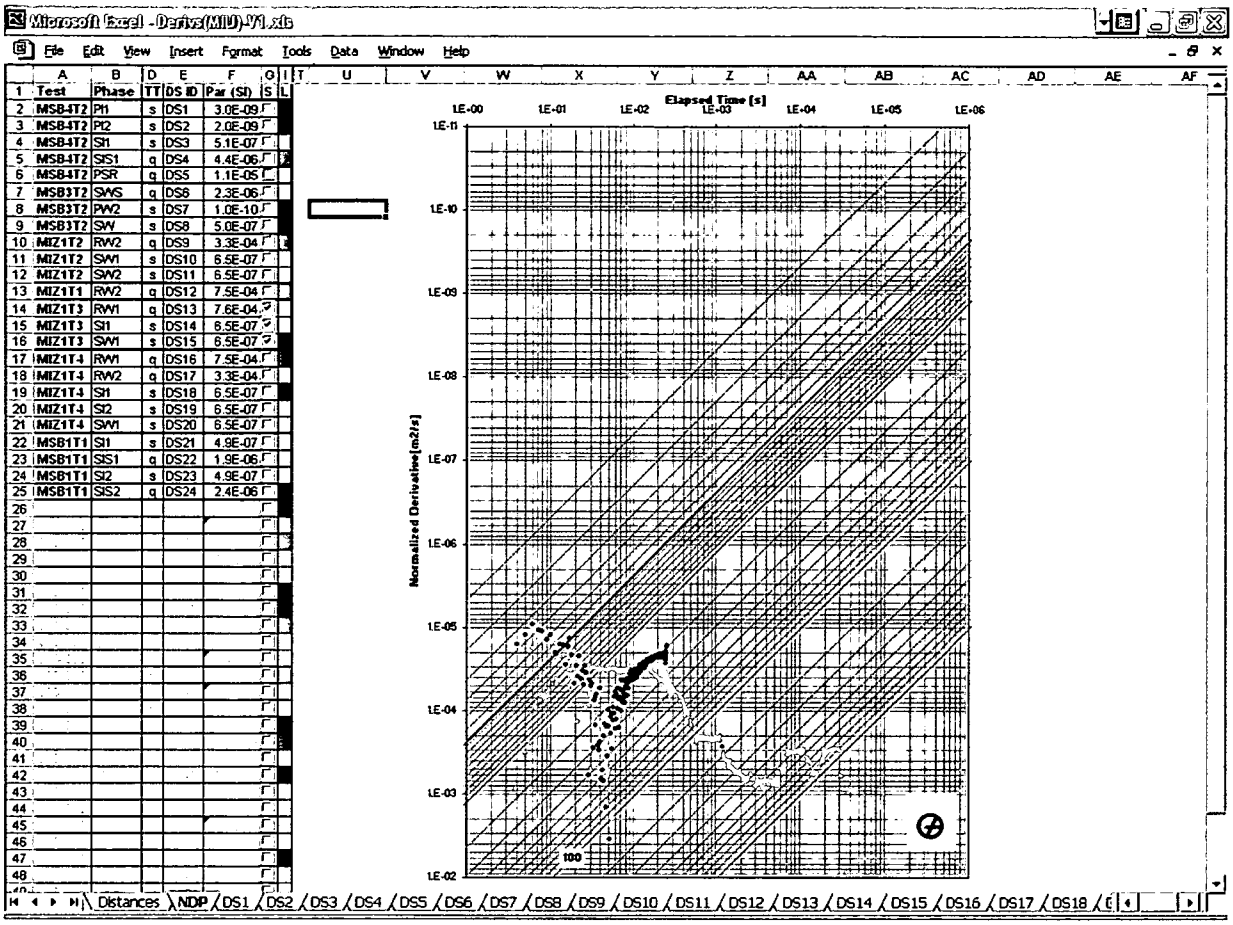

	Test	Phase	TT	DS ID	Par (SI)
2	MSB4T2	PI1	s	DS1	3.0E-09
3	MSB4T2	PI2	s	DS2	2.0E-09
4	MSB4T2	SI1	s	DS3	5.1E-07
5	MSB4T2	SIS1	q	DS4	4.4E-06
6	MSB4T2	PSR	q	DS5	1.1E-05
7	MSB3T2	SWS	q	DS6	2.3E-06
8	MSB3T2	PW2	s	DS7	1.0E-10
9	MSB3T2	SW	s	DS8	5.0E-07
10	MIZ1T2	RW2	q	DS9	3.3E-04
11	MIZ1T2	SW1	s	DS10	6.5E-07
12	MIZ1T2	SW2	s	DS11	6.5E-07
13	MIZ1T1	RW2	q	DS12	7.5E-04
14	MIZ1T3	RW1	q	DS13	7.6E-04
15	MIZ1T3	SI1	s	DS14	6.5E-07
16	MIZ1T3	SW1	s	DS15	6.5E-07
17	MIZ1T4	RW1	q	DS16	7.5E-04
18	MIZ1T4	RW2	q	DS17	3.3E-04
19	MIZ1T4	SI1	s	DS18	6.5E-07
20	MIZ1T4	SI2	s	DS19	6.5E-07
21	MIZ1T4	SW1	s	DS20	6.5E-07
22	MSB1T1	SI1	s	DS21	4.9E-07
23	MSB1T1	SIS1	q	DS22	1.9E-06
24	MSB1T1	SI2	s	DS23	4.9E-07
25	MSB1T1	SIS2	q	DS24	2.4E-06

Figure 3-6 MIZ1: T3 Hydraulic Test Interpretation

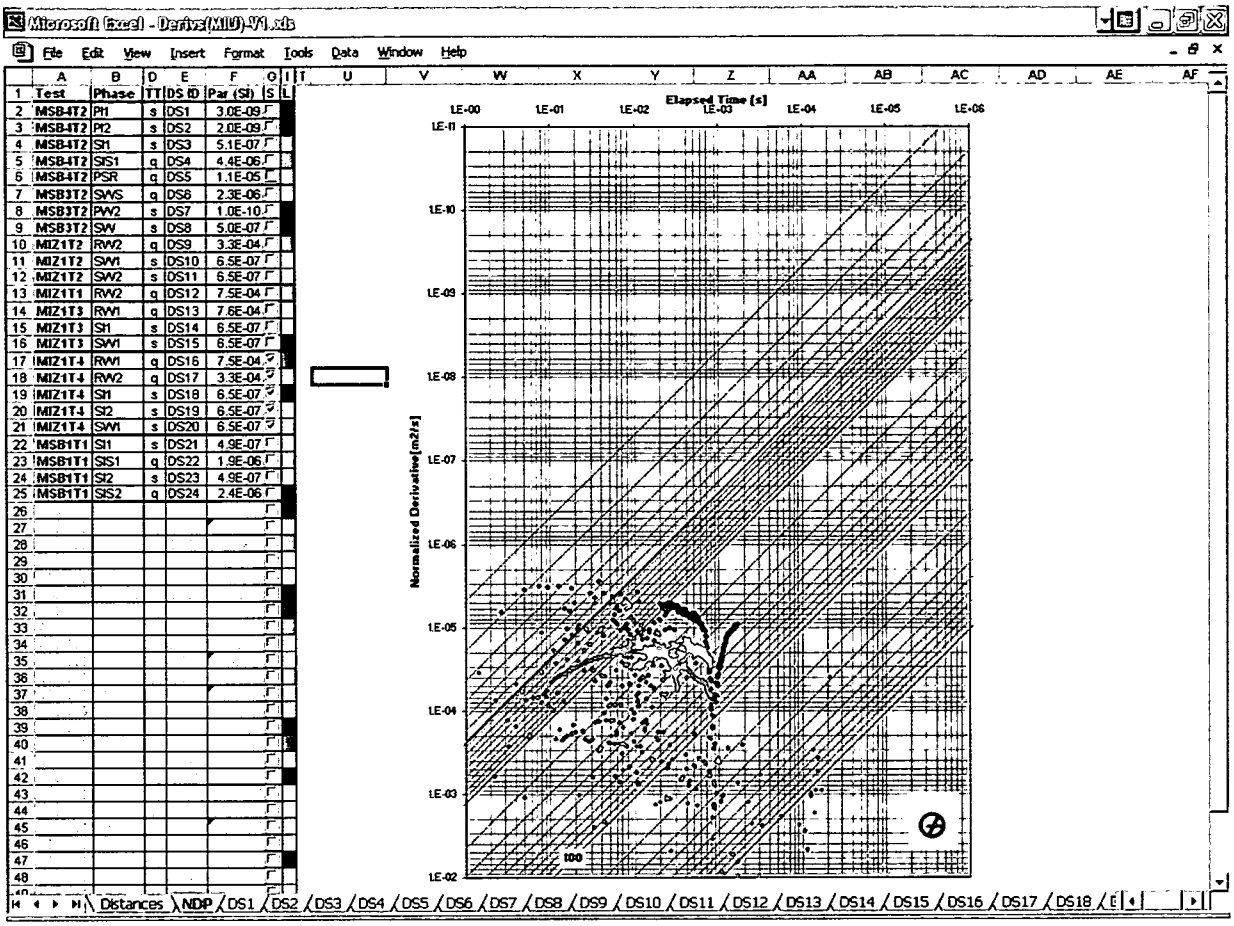

	Test	Phase	TT	DS ID	Par (SI)
2	MSB4T2	PH	s	DS1	3.0E-09
3	MSB4T2	PI2	s	DS2	2.0E-09
4	MSB4T2	SI1	s	DS3	5.1E-07
5	MSB4T2	SIS1	q	DS4	4.4E-06
6	MSB4T2	PSR	q	DS5	1.1E-05
7	MSB3T2	SWS	q	DS6	2.3E-06
8	MSB3T2	PW2	s	DS7	1.0E-10
9	MSB3T2	SW	s	DS8	5.0E-07
10	MIZ1T2	RW2	q	DS9	3.3E-04
11	MIZ1T2	SW1	s	DS10	6.5E-07
12	MIZ1T2	SW2	s	DS11	6.5E-07
13	MIZ1T1	RW2	q	DS12	7.5E-04
14	MIZ1T3	RW1	q	DS13	7.6E-04
15	MIZ1T3	SI1	s	DS14	6.5E-07
16	MIZ1T3	SW1	s	DS15	6.5E-07
17	MIZ1T4	RW1	q	DS16	7.5E-04
18	MIZ1T4	RW2	q	DS17	3.3E-04
19	MIZ1T4	SI1	s	DS18	6.5E-07
20	MIZ1T4	SI2	s	DS19	6.5E-07
21	MIZ1T4	SW1	s	DS20	6.5E-07
22	MSB1T1	SI1	s	DS21	4.9E-07
23	MSB1T1	SIS1	q	DS22	1.9E-06
24	MSB1T1	SI2	s	DS23	4.9E-07
25	MSB1T1	SIS2	q	DS24	2.4E-06

Figure 3-7 MIZ1:T4 Hydraulic Test Interpretation

2.1 Task 2.2: MIU Hydrostructural Synthesis

Golder Associates will assist JNC by carrying out a review of the hydrostructural model developed by JNC/Tono for the site of the MIU Shaft. This review was supported by a detailed interpretation of each of the MSB and MIZ-1 testing sections. Table 3-2 and Figure 3-8 through Figure 3-11 provided illustrative examples of these analyses, from the MIZ-1:T1 RW test..

Table 3-3 Flow Dim Data Sheet, MIZ-1:T1/RW

TEST ANALYSIS REPORT			17.12.2003
IDENTIFICATION			
Site name			: MIU
Well name			: MIZ
Interval name			: T1
Event name			: RW
Date			: xx.xx.xx
Input file name			: Z11RW2-V1.RPT
WELL PARAMETERS			
Well depth		[m brp]	: xxx
Reference point elevation		[m asl]	: xxx
Wellbore radius	(rw)	[m]	: 5.70E-02
Interval length	(h)	[m]	: 1.00E+01
TESTPARAMETERS			
Production/Injection time	(tP)	[h]	: 17.5
Flow rate	(q)	[l/min]	: 4.50E+01
Test duration	(tt)	[h]	: 1.95E+01
FLUID AND FORMATION PARAMETERS			
Viscosity	(æw)	[Pa s]	: 1.20E-03
Total compressibility	(ct)	[1/Pa]	: 1.00E-09
Porosity	(n)	[-]	: 1.00E-02
MODEL ASSUMPTIONS			
Flow model			: Composite
Boundary conditions			: Constant rate
Well type			: Source
Superposition type			: Buildup
TEST RESULTS			
Transmissibility	(T)	[m3]	: 3.25E-09
Transmissivity	(Th)	[m2/s]	: 2.66E-02
Storage	(S)	[m/Pa]	: 1.00E-10
Storativity	(Sh)	[-]	: 9.81E-07
Wellbore storage coefficient	(C)	[m3/Pa]	: 8.21E-06
Inner shell flow dimension	(n1)	[-]	: 2.00E+00
Outer shell flow dimension	(n2)	[-]	: 2.00E+00
Discontinuity radius	(r1)	[m]	: 8.47E+03
Mobility ratio	(sg)	[-]	: 3.64E+01
Storativity ratio	(sr)	[-]	: 1.13E+05

Interpret 2003

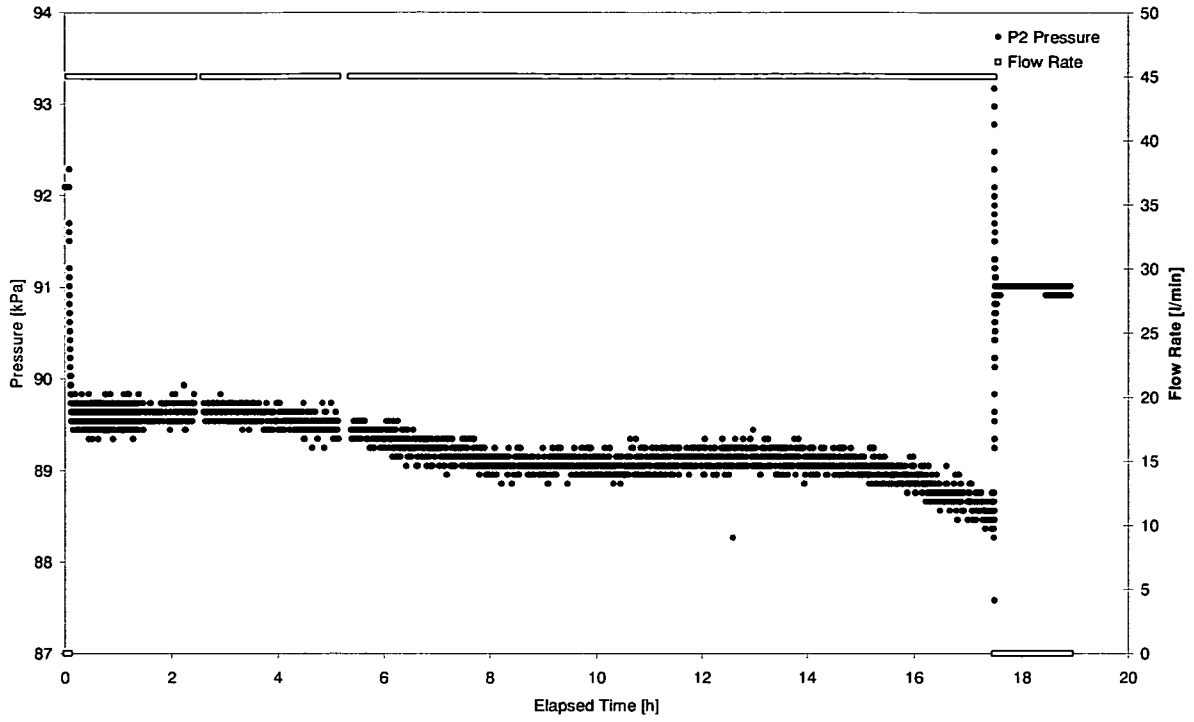

Figure 3-8 Borehole MIZ; Test 1; RW phase; Cartesian plot

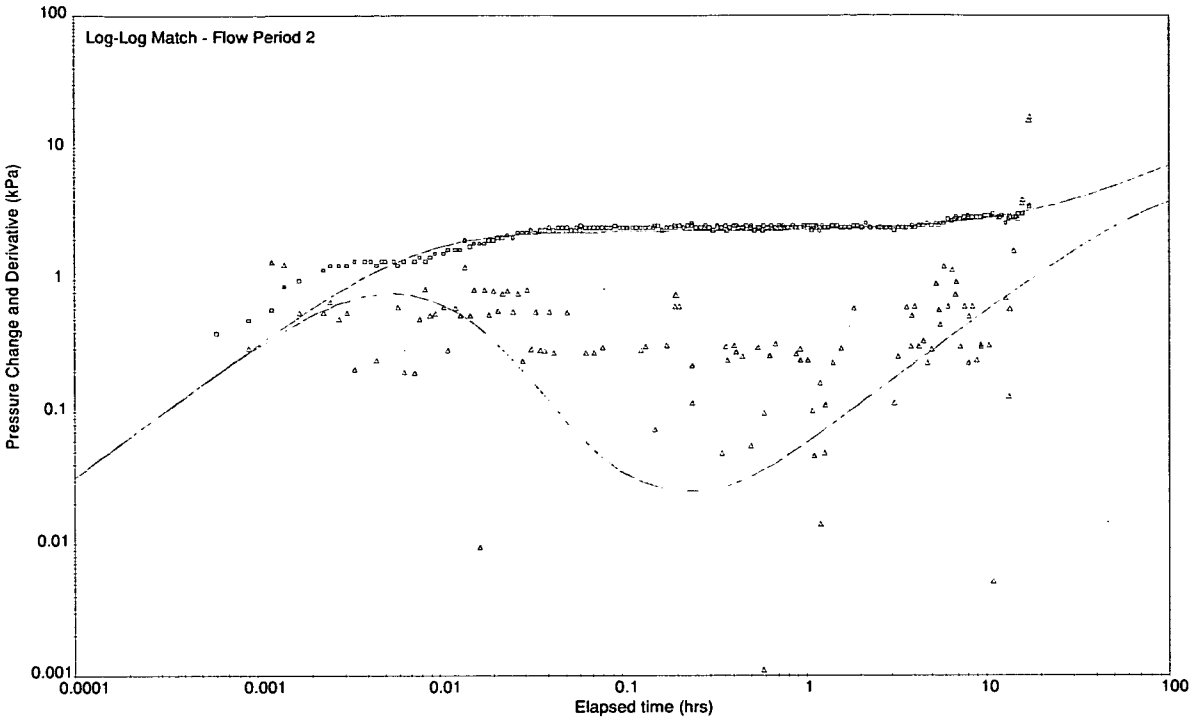

Figure 3-9 Borehole MIZ; Test 1; RW phase; Log-Log plot

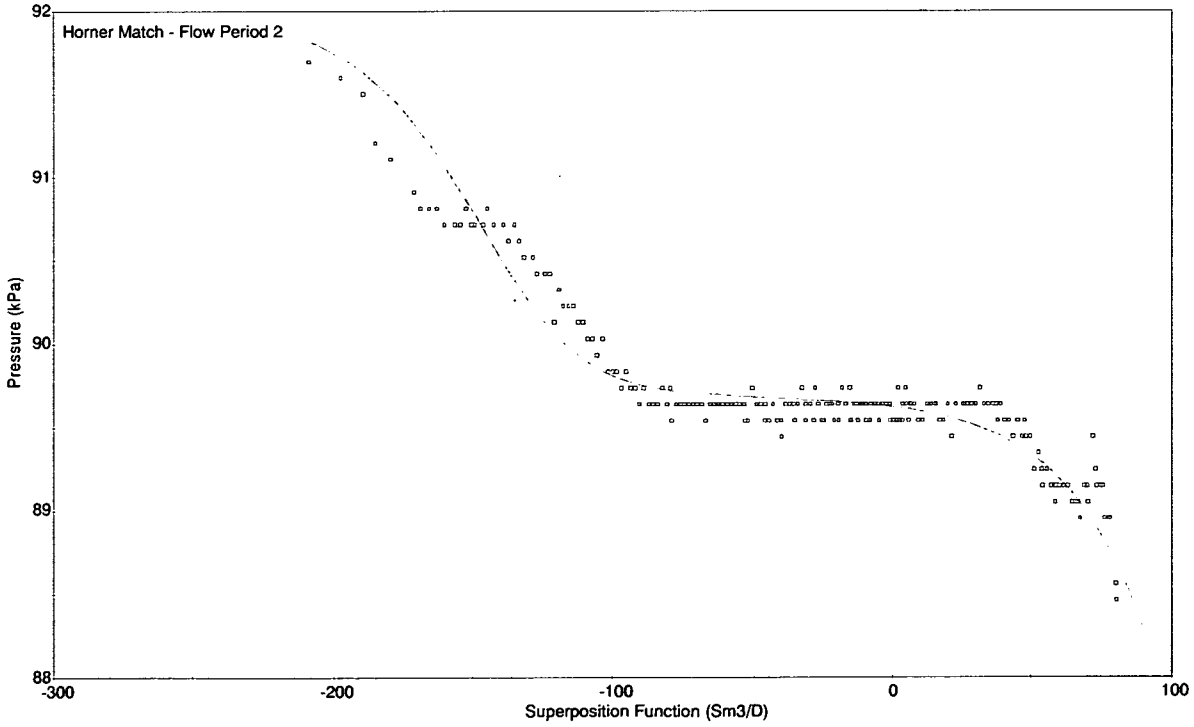

Figure 3-10 Borehole MIZ; Test 1; RW phase; Horner plot

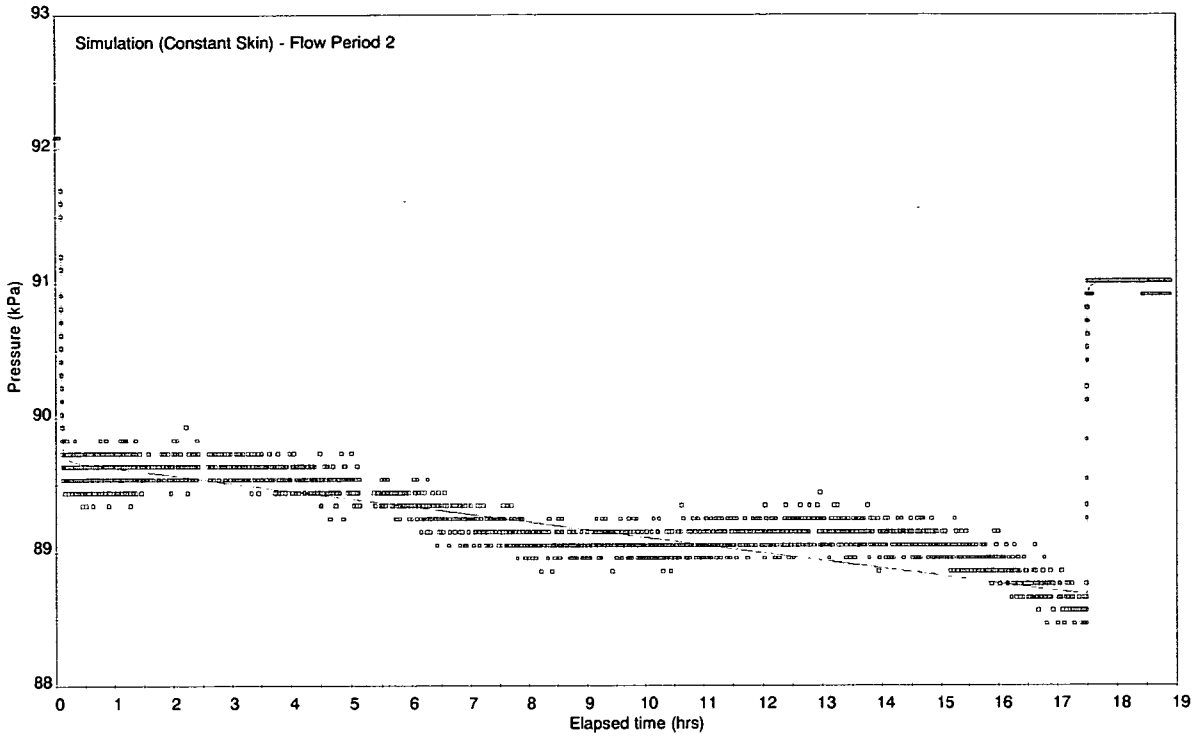

Figure 3-11 Borehole MIZ; Test 1; RW phase; Simulation

3.2 Task 2.3: MIU DFN Modeling

During H-15, JNC is initiating the sinking of the MIU shaft at the Mizunami rock lab. Golder Associates assisted JNC by simulating the sinking of the shaft, and the concomitant grouting activities using the FracMan/MAFIC package.

These simulations utilized the DFN model developed for JNC based on the JNC "local scale" (Dershowitz et al., 2003). The simulations directly implement the expected time history of shaft sinking, and a possible grouting scenario. Boundary conditions and material properties are defined to be similar to those used in continuum modeling by JNC/Tono. The model includes JNC planned monitoring boreholes and intervals.

3.2.1 DFN Model Implementation

Figure 3-12 shows the model region used for the DFN grouting simulations. The model volume extends from the surface to a depth of 2000 m. Figure 3-13 illustrates the separation between the granite (DFN) portion of the model, and the continuum (EPM) portion of the model. The region

between the topographic surface and the unconformity surface are represented by continuum elements representing the sediments of the Mizunami Group.

The UHFD_bottom.ts separates the Toki granite in two zones. The highly fracture zone of the Toki granite lies between the unconformity.ts and the UHFD_bottom.ts and the moderately fractured Toki granite lies between the UHFD_bottom.ts and the H15bottom.ts .

Figure 3-14 shows the EPM implementation of the sediments of the Mizunami Group which overlying the Toki Granite. Holes represent areas where the granite reaches the topographic surface. The grid box region is 50 by 50 by 5.

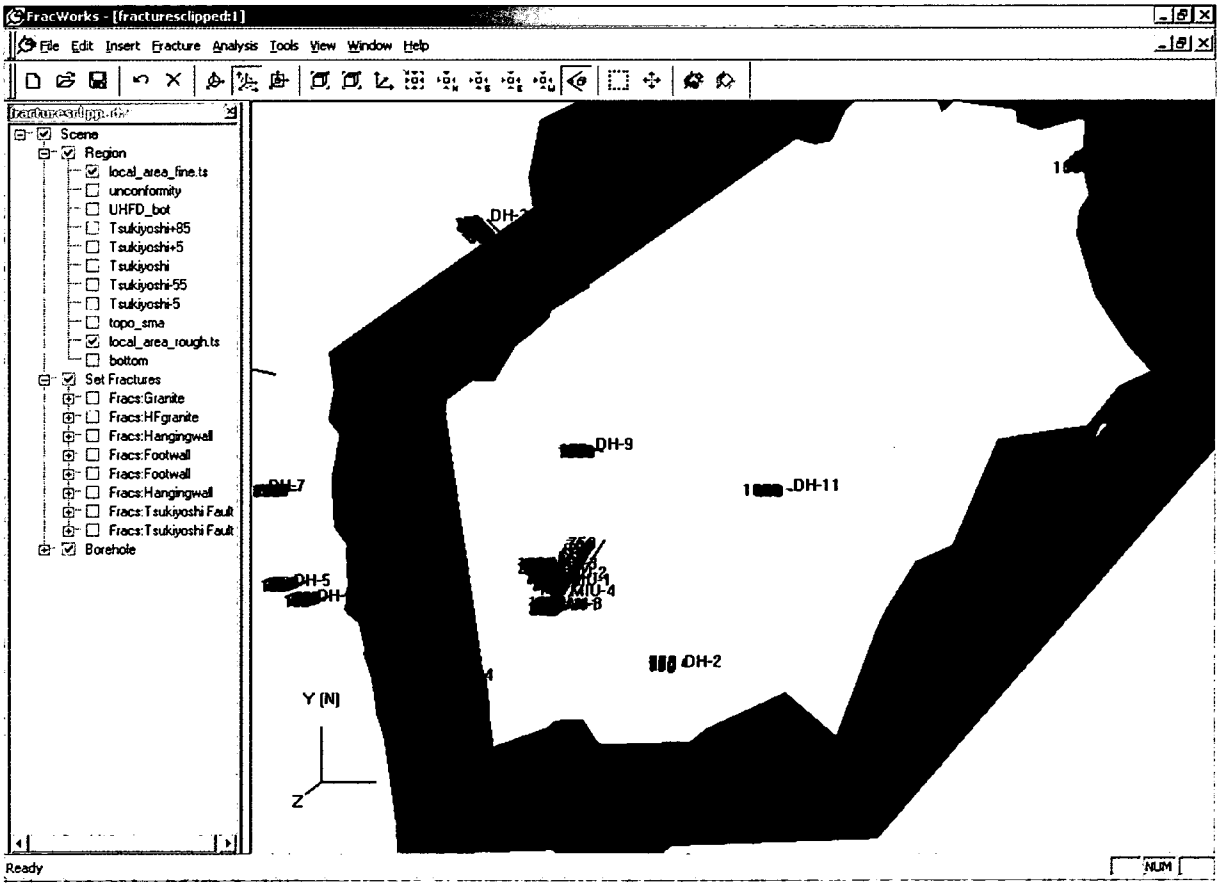

Figure 3-12 MIU Shaft DFN Model Region. The borehole in the NE corner is DH-10

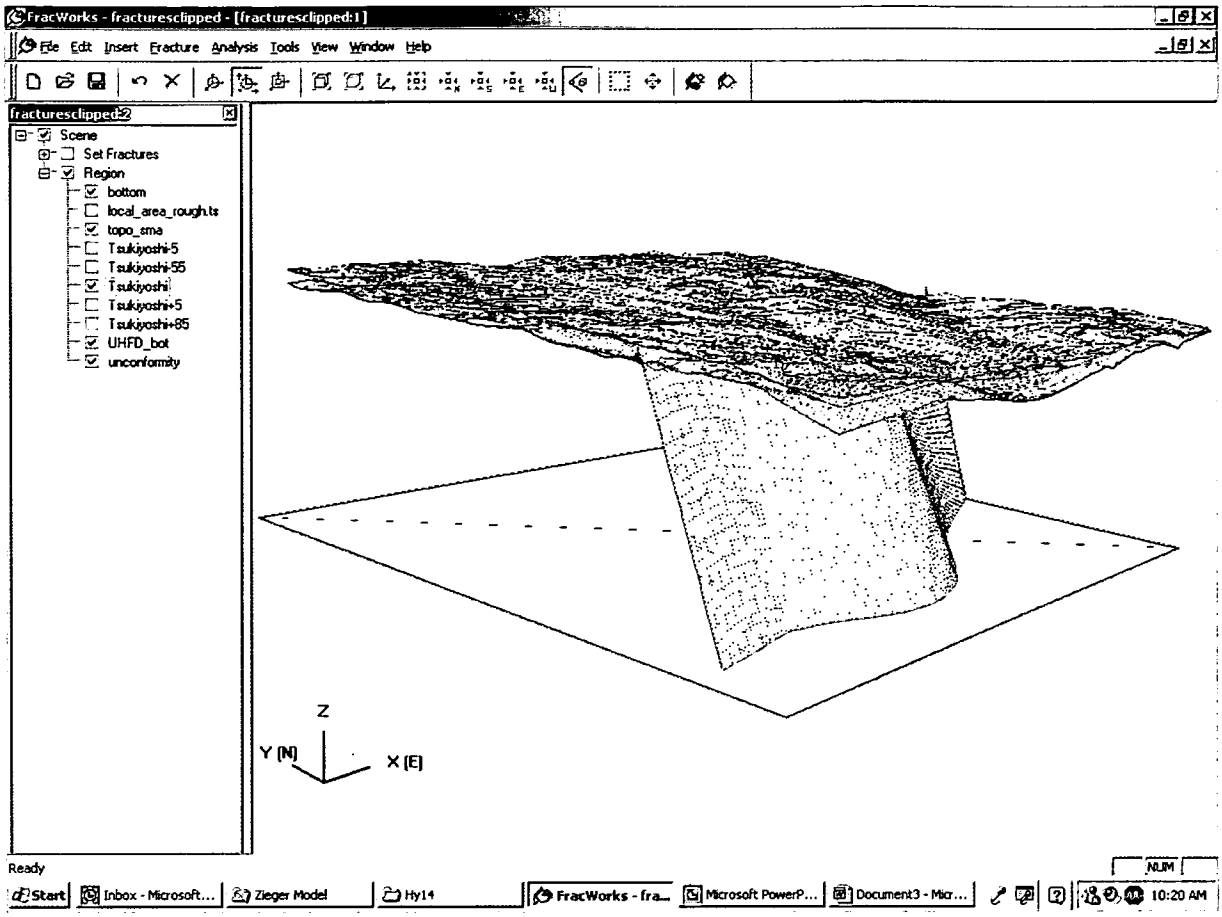

Figure 3-13 H15 Model Stratigraphic Surfaces. (white = topographic surface, topo.ts; red = unconformity, unconformity.ts; turquoise = bottom of highly fractured granite, UHFD_bottom.ts; orange = tsukiyoshi fault, tsukiyoshi.ts; pale green = bottom, H15bottom.ts)

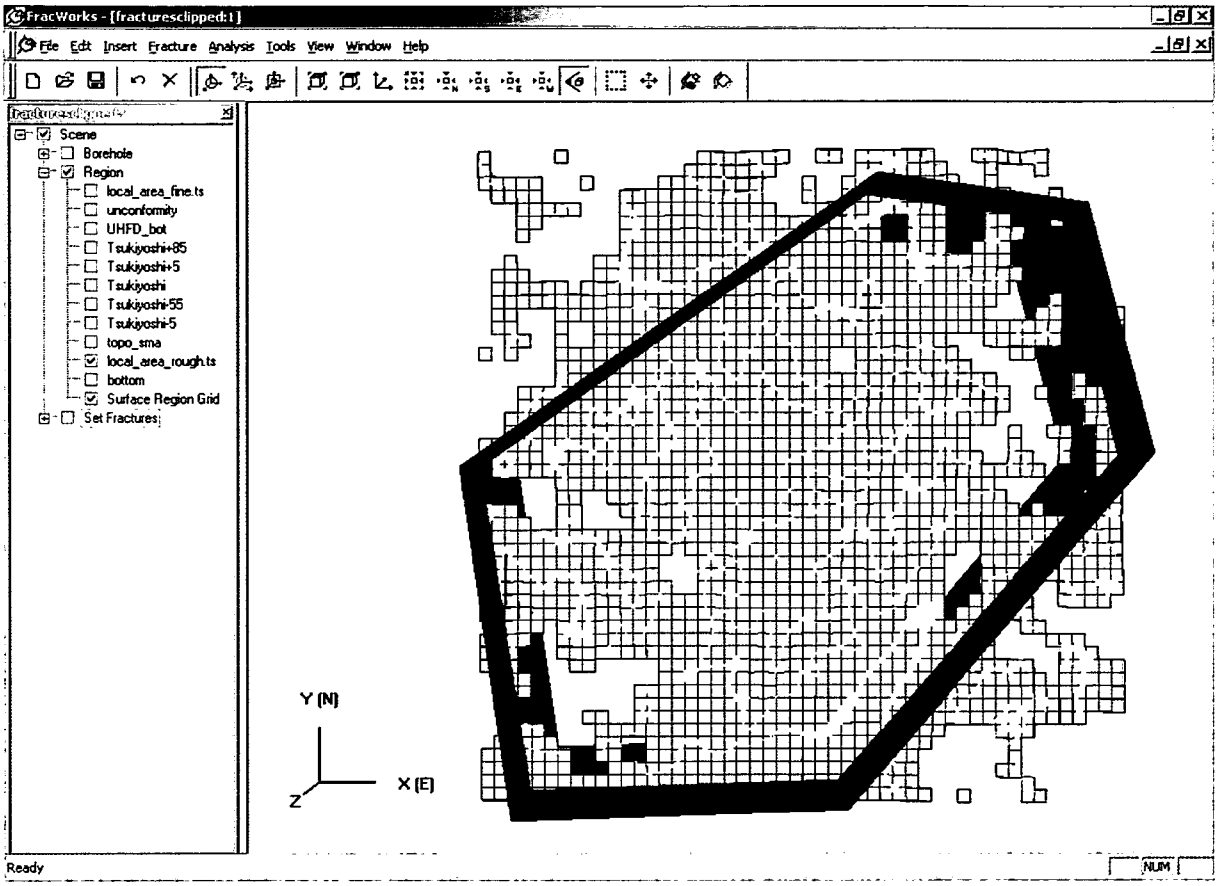

Figure 3-14 Mizumani Group Continuum Elements

Figure 3-15 illustrate the deterministic faults included in the H15 DFN model. Figure 3-16 illustrates the background fractures. The properties of background fractures are summarized in

Table 3-4. For more information on these features, see Dershowitz et al. (2003).

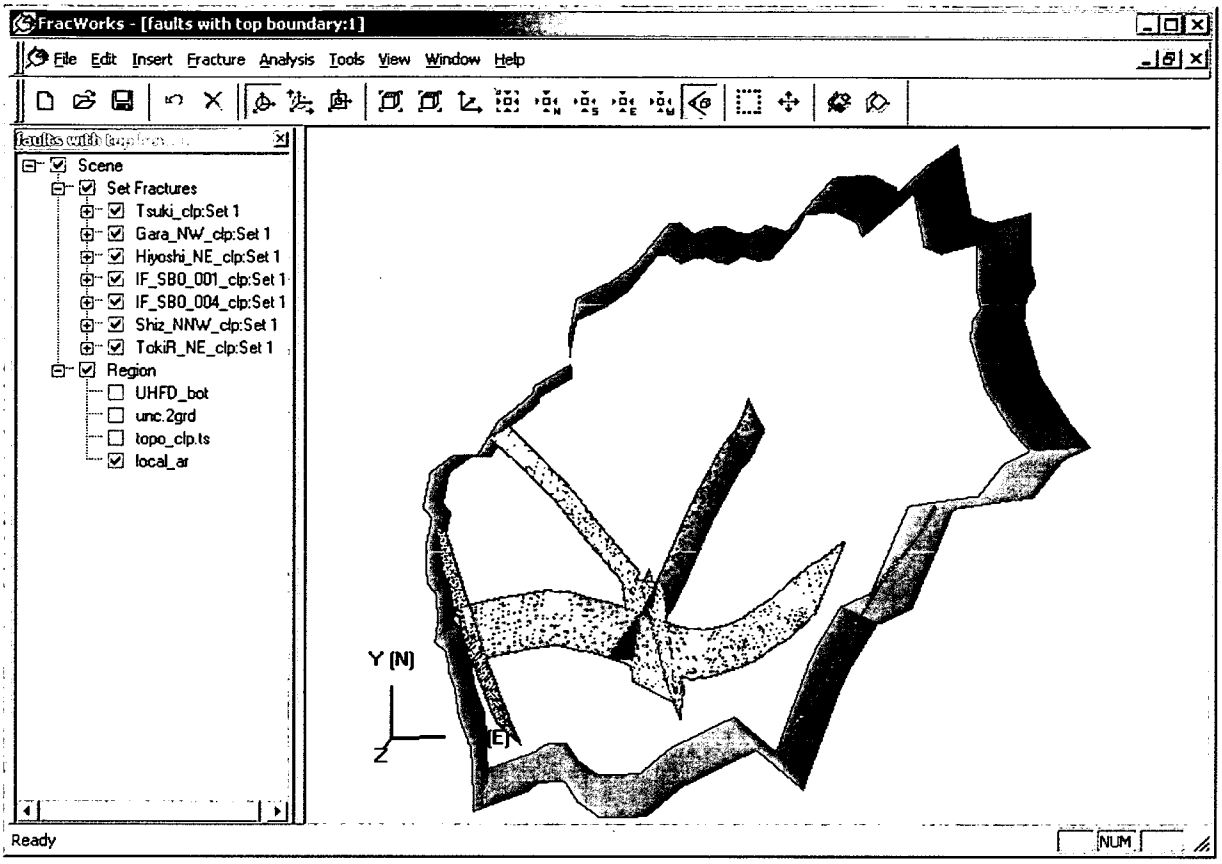

Figure 3-15 MIU Shaft DFN Model Deterministic Faults

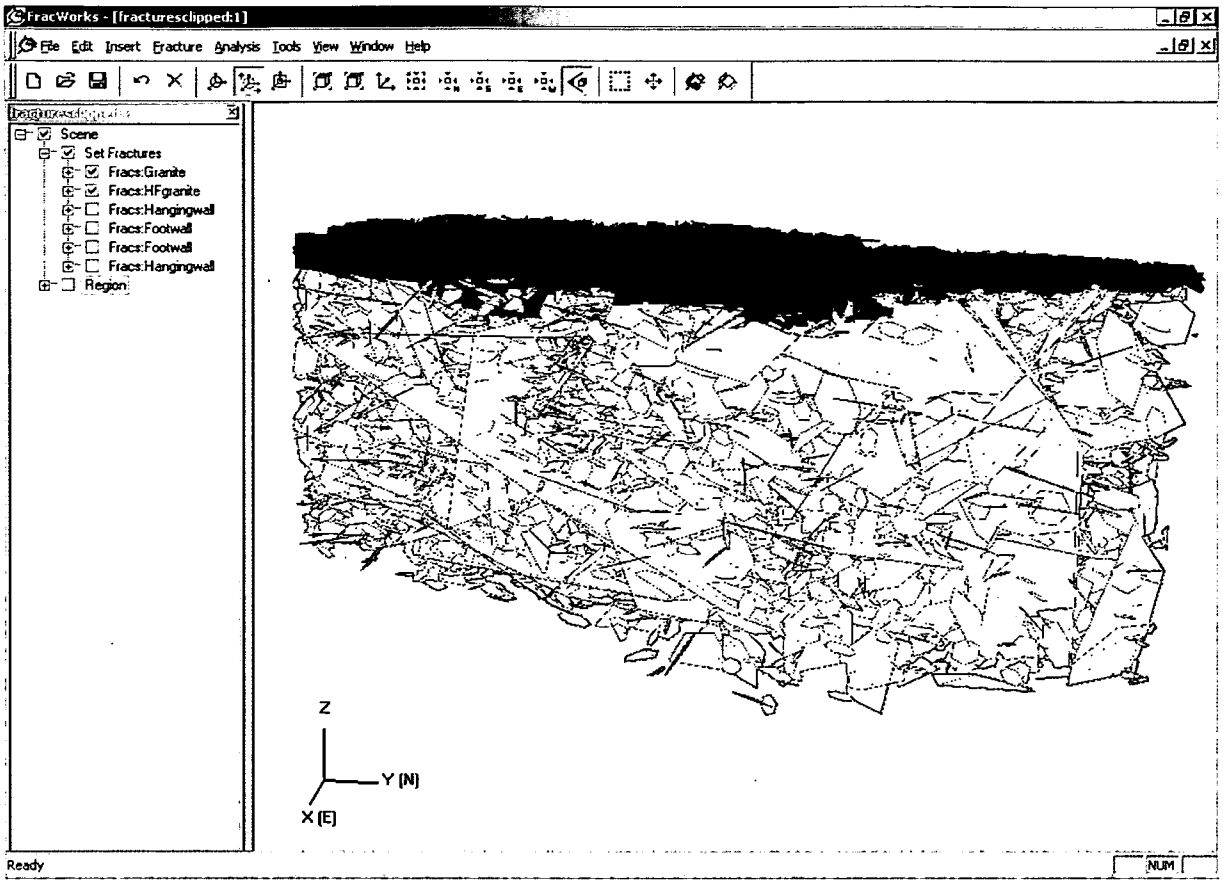

Figure 3-16 Background Fracturing in Toki Granite and Highly Fractured Granite Zones

The Tsukiyoshi fault was implemented using the following procedure.

1. The Tsukiyoshi fault is implemented directly as non-planar fracture surface, with constant transmissivity of 10^{-9} m^2/s (see Figure 3-13).
2. Fractures are generated in the hangingwall highly fractured zone, in the hangingwall portion of the Toki granite, and the hangingwall portion of the highly fractured zone.
3. These 3 sets of "hangingwall" fractures are all truncated at the Tsukiyoshi fault surface.
4. Fractures are generated in the footwall highly fractured zone, in the footwall portion of the Toki granite, and the footwall portion of the highly fractured zone.
5. These 3 sets of "footwall" fractures are all truncated at the Tsukiyoshi fault surface.

Due to the truncation of the footwall and hangingwall fractures on the same surface, these fractures are not connected hydraulically except through the low permeability Tsukiyoshi fault surface. This provides a significant flow barrier effect.

This algorithm is illustrated Figure 3-17 and Figure 3-18. Figure 3-17 shows the hangingwall highly fracture zone and footwall highly fractured zone fractures. Figure 3-18 shown there fractures after truncation against the Tsukiyoshi fault surface (Figure 3-13).

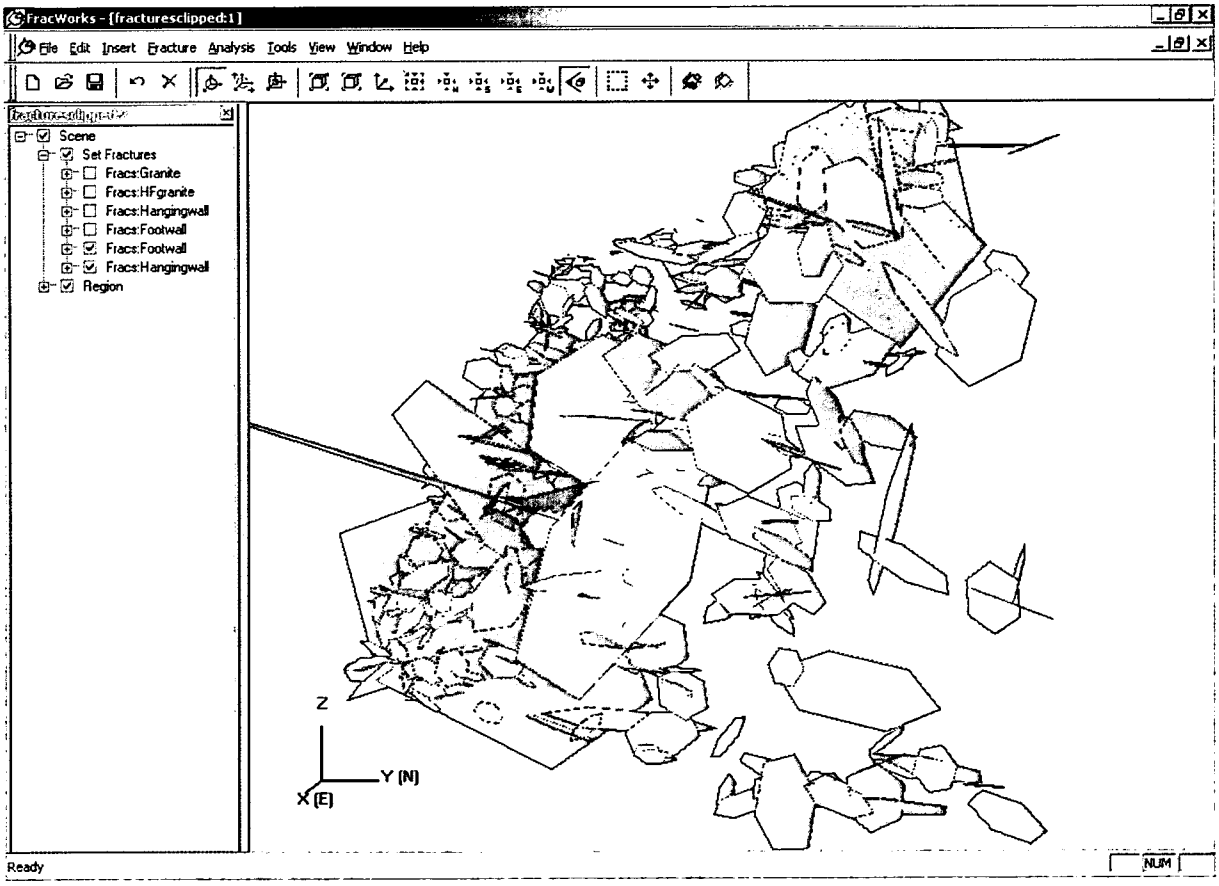

Figure 3-17 Hangingwall (red) and Footwall (green) highly fractured zone fractures

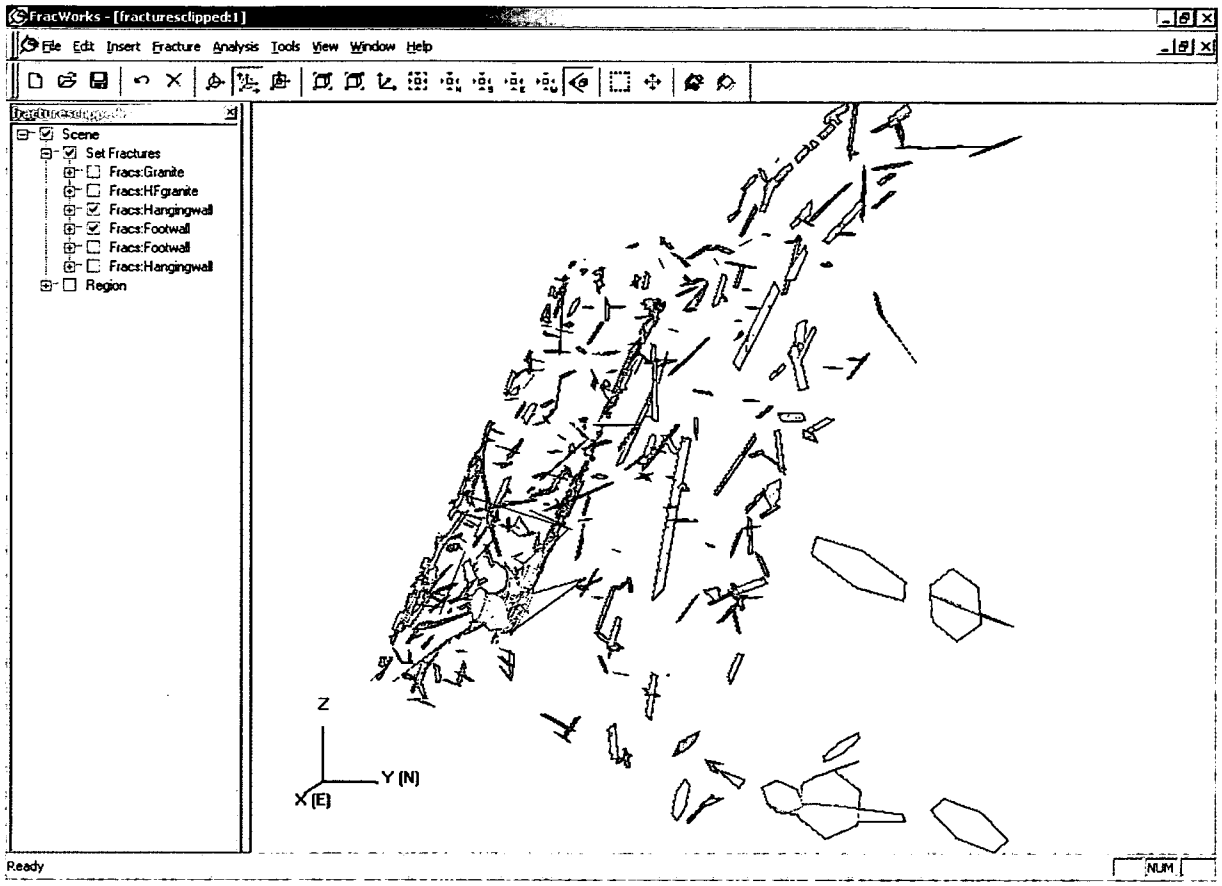

Figure 3-18 Hanginwall (red) and Footwall (green) highly fractured zone fractures terminated on different side of the Tsukiyoshi Fault

Table 3-4 H14 MIU-4 Model Fracture Generation Parameters

Spatial Model	Enhanced Baecher Model
Generation Region	Toki Granite = Between wgran_3.ts and bottom.ts Highly Fractured Zone = Between unc2_3.ts and upfrab.ts Hangingwall = Between tsuki2_3+5.ts and tsuki2_3+85.ts Footwall = Between tsuki2_3-5.ts and tsuki2_3-55.ts
Orientation (pole)	Bootstrap Orientation, fisher k = 100 Toki Granite = TOK1234T.ors Highly Fractured Zone = HFZ1234T.ors Hangingwall = HAN1234T.ors Footwall = FOT1234T.ors
Size (m)	Truncated Power Law, Xo = 25, b = 3.6, Xmax = 3000 Toki Granite =Xmin = 400 Highly Fractured Zone =Xmin = 200 Hangingwall =Xmin = 50 Footwall =Xmin = 50
Truncated P_{32} Intensity (m^2/m^3)	Toki Granite = 0.00852 m^2/m^3 Highly Fractured Zone = 0.02362 m^2/m^3 Hangingwall = 0.04198 m^2/m^3 Footwall = 0.07851 m^2/m^3
Transmissivity (m^2/s)	Lognormal Distribution Toki Granite = Log mean = -6.0, Log stdev = 0.5 Highly Fractured Zone = Log mean = -6.5, Log stdev = 0.5 Hangingwall = Log mean = -5.0, Log stdev = 0.7 Footwall = Log mean = -5.0, Log stdev = 0.7
Fracture Storativity (-)	$S = 0.46*T^{1/2}$
Aperture (m)	$e_t = 2*T^{1/2}$
Clipping surface	Toki Granite = Upper surface = upfrab_3.ts Highly Fractured Zone = None Hangingwall = Upper surface = unc2_3.ts, Lower surface = tsuki_3.ts Footwall = Upper surface = unc2_3.ts and tsuki_3.ts

3.2.2 Shaft Construction and Grouting Simulations

3.2.2.1 MIU Shaft Construction Assumptions

The MIU shaft is illustrated in Figure 3-19. The assumed schedule for MIU construction is illustrated in Figure 3-20.

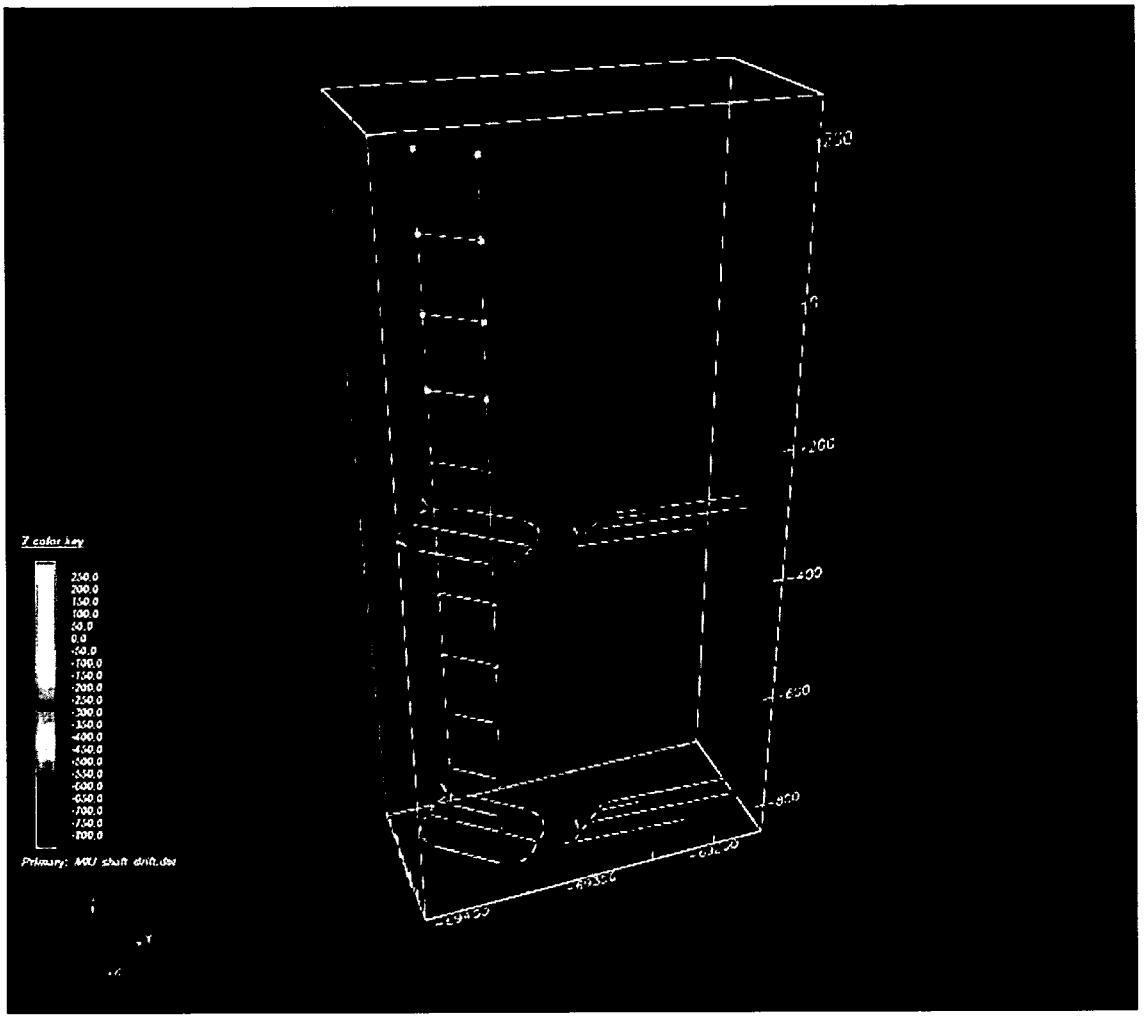

Figure 3-19 MIU Shaft (after JNC, 2003)

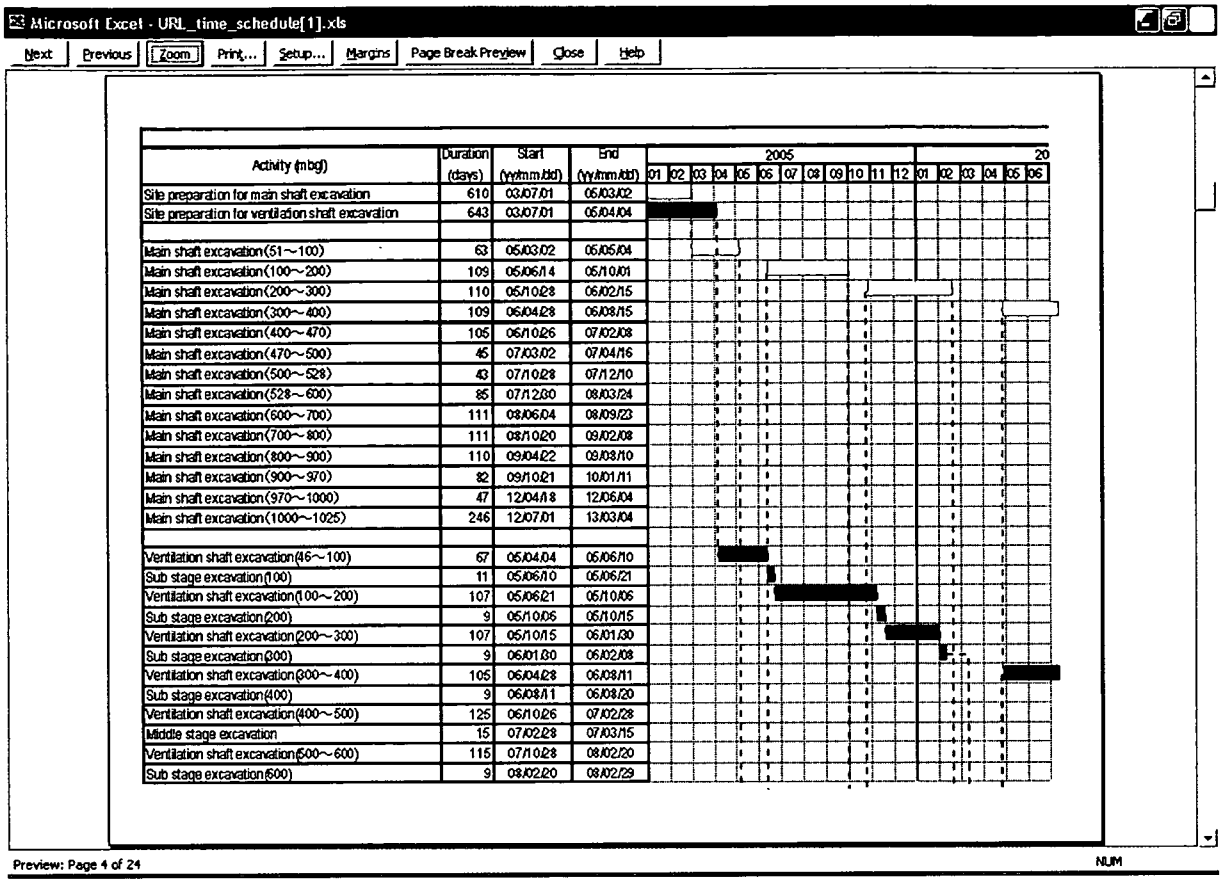

Figure 3-20 Assumed MIU Shaft Construction Schedule

3.2.3 Grouting Simulation

FracMan/EdMesh simulates grouting using an algorithm similar to that which occurs in nature (Figure 3-20). The shaft construction is simulated in stages. For each stage, the grouting simulation proceeds as follows. First, the fractures intersecting the shaft stage are identified in the DFN model, and the ungrouted flow into the shaft is estimated. A required grout volume (in bags) is then estimated based on this ungrouted flow, and a grout injection borehole array is designed. Grout is then injected to thee fractures connected to the simulated grout injection borehole array. Grout is injected into fractures successively with priority given on the basis of fracture aperture – largest fractures first (Figure 3-21). The grout injection then progresses following the "path of least resistance" from fractures connected to the grout injection borehole into the chain of interconnected fractures, until the total volume of grout is taken up. The

grouted portions of fractures are then assigned a transmissivity of 10^{-10} m^2/s. A grouted fracture network is illustrated in Figure 3-22.

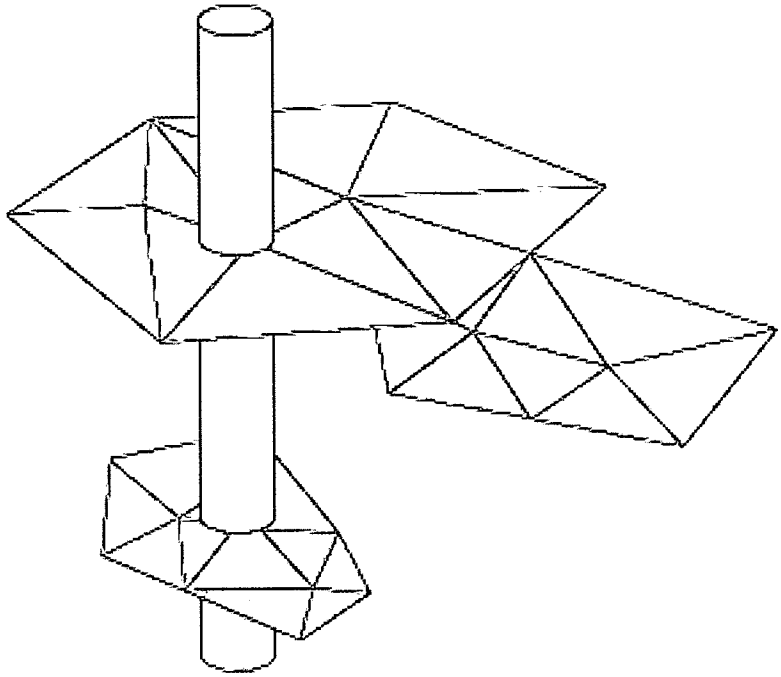

Figure 3-21 Grouting Algorithm.

This simple model for shaft grouting is controlled by fracture geometry, and the flow of grout into the fractures is defined by a simple heuristic. The effect of injection pressure, grout theology, and fracture microstructure are not considered explicitly. Instead, they are considered implicitly through the grout volume injection boundary condition.

In the current study, gel was injected to the Toki granite based on the grout construction schedule showed in Figure 3-20.

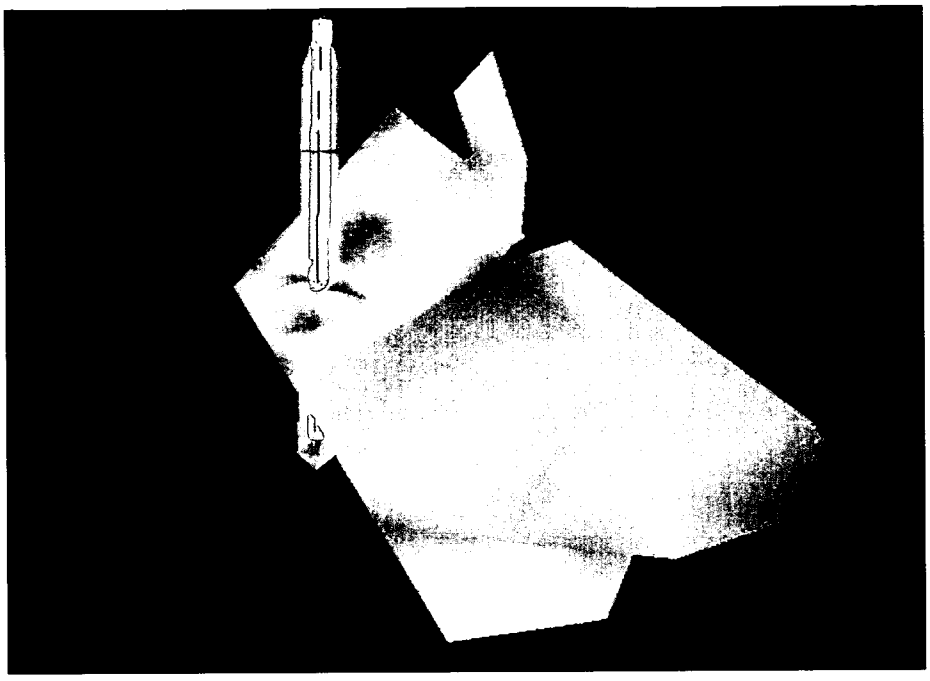

Figure 3-22 Example Visualization of Grouted portions of fractures connected to Grouting Borehole

4. CONCLUSION

During Heisei-15, Golder Associates developed and documented substantial advances in radioactive waste management technology for JNC. The major accomplishments of H-15 include:

- Analysis of hydraulic interference, tracer dilution, and tracer tests from the TRUE-BSC project to improve characterization of Structure #19 for sorbing tracer experiments planned for H-16
- Development of fracture flow, transport, and retention hypotheses to be tested in the TRUE-BSC project.
- Interpretation of hydraulic tests from the MIU site, including detailed analyses of MSB series tests, and MIZ-1.
- Preliminary simulation of hydraulic interference response to construction of the MIU shaft.

5. REFERENCES

Andersson, P., et al., 2002: "Final Report of the TRUE Block Scale project TR-02-13 part 1", SKB.

Andersson, P., J. Byegård, T. Doe, J. Hermanson, P. Meier, E.-L. Tullborg, and A. Winberg, 2002. "TRUE Block Scale Project Final Report – 1. Characterization and model development", Swedish Nuclear Fuel and Waste Management Company (SKB), Technical Report TR-02-13. SKB, Stockholm

Dershowitz, W and K Klise, 2003. FracWorks XP User Documentation, V. 0.25. Golder Associates, Inc, Seattle.

Dershowitz, W., A. Winberg, J. Hermanson, J. Byegård, E.L. Tullborg, P. Andersson, and M. Mazurek, 2003. A Semi-synthetic Model of Block Scale Conductive Structures at the Äspö Hard Rock Laboratory. SKB, Stockholm.

Dershowitz, W., M. Uchida, and K. Klise, 2002. Predictive Simulation and Evaluation, TRUE Block Scale Project. SKB, Stockholm.

Dershowitz, W., Winberg, A., Hermanson, J., Byegard, J., Tullborg, E-L., Andersson, P., Mazurek, M., 2003: "A Semi-Synthetic Model of Block Scale Conductive Structures at the Aspo Hard Rock Laboratory", Aspo Task Force Task 6C Report.

Foxford, T., B. Dershowitz, E. Sudicky, and D. Shuttle, 2002. PAWorks User Docuemtation, v. 1.65. Golder Associates, Inc., Seattle

Hermanson, J. and T. Doe., 2000: "TRUE Block Scale Tracer test stage, March '00 structural and hydraulic model based on borehole data from KI0025F03", Swedish Nuclear Fuel and Waste Management Company, Aspo HRL International Progress Report IPR-00-34.

Miller, I, G. Lee, and W. Dershowitz, 2002. MAFIC User Documentation, v. 1.713. Golder Associates, Inc., Seattle.